CHALMERS
UNIVERSITY OF TECHNOLOGY

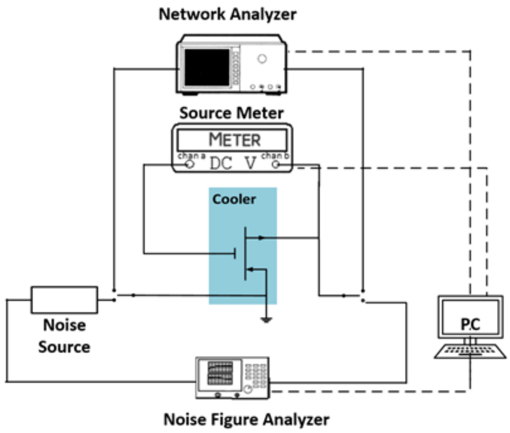

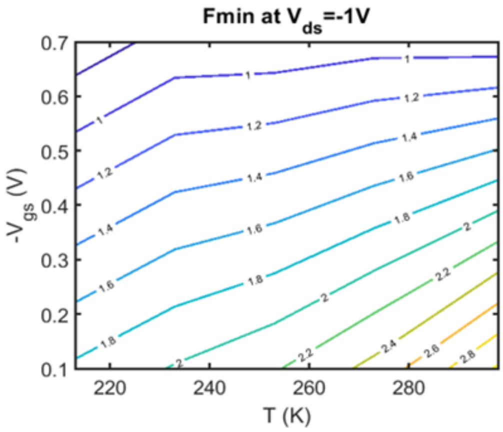

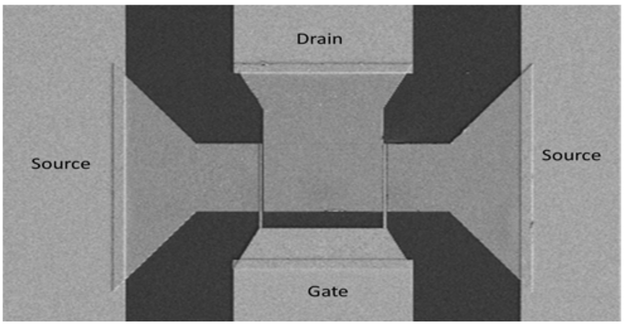

Characterisation of high-frequency noise in graphene FETs at different ambient temperatures

Master's thesis in Applied Physics

Junjie Li

Department of Microtechnology and Nanoscience
CHALMERS UNIVERSITY OF TECHNOLOGY
Gothenburg, Sweden 2019

MASTER'S THESIS 2019

Characterisation of high-frequency noise in graphene FETs at different ambient temperatures

Junjie Li

CHALMERS
UNIVERSITY OF TECHNOLOGY

Terahertz and Millimetre Wave Laboratory
Department of Microtechnology and Nanoscience
CHALMERS UNIVERSITY OF TECHNOLOGY
Gothenburg, Sweden 2019

Characterisation of high-frequency noise in graphene FETs at different ambient temperatures

Supervisor: Xinxin Yang, Department of Microtechnology and Nanoscience
Examiner: Jan Stake, Department of Microtechnology and Nanoscience

Master's Thesis 2019
Terahertz and Millimetre Wave Laboratory
Department of Microtechnology and Nanoscience
Chalmers University of Technology
SE-412 96 Gothenburg, Sweden
Telephone +46 31 772 1000

Cover:
Top left: Schematic block diagram of thermal noise measurement setup for 50 Ω termination method.
Top right: F_{min} in decibel versus temperature at 6.5 GHz and drain bias of -1 V
Bottom: SEM image of a GFET

Typeset in LaTeX
Gothenburg, Sweden 2019

Characterisation of high-frequency noise in graphene FETs at different ambient temperatures
Junjie Li
Terahertz and Millimetre Wave Laboratory
Department of Microtechnology and Nanoscience
Chalmers University of Technology

Abstract

Graphene is a promising channel material for high-frequency field-effect transistors, owing to its intrinsically high carrier velocity and purely two-dimensional structure. At high frequencies, the noise originated in device itself, especially the thermal noise, becomes very crucial for the performance of transistors. The thermal noise can be influenced by ambient temperature or self-heating due to high drain bias. This motivates the study of the effect of temperature on the noise performance of graphene field-effect transistors (GFETs).

In this thesis, the results on high-frequency noise characterisation and modelling of the GFETs at different temperature and bias conditions are presented. The basic idea and main procedures of high-frequency noise modelling are based on Pospieszalski's noise model. Two different high-frequency noise characterisation techniques, i.e., the Y-factor and cold-source methods, and two calculation methods of high-frequency noise parameters, i.e., the source-pull and 50 Ω impedance termination (F_{50}) methods, have been analysed and discussed. The high-frequency noise of the GFETs at an ambient temperature range from -60 °C to 25 °C is presented. The minimum noise figure (F_{min}) of the GFETs decreases with the drain bias and saturates above approximately -1 V due to the carrier mobility saturation in the channel. The noise performance shows a rather strong dependence on both temperature and gate bias mainly due to the change of carrier density and the contact resistance. The minimum noise figure (F_{min}) is 1.2 dB at 6.5 GHz at room temperature, which is comparable with that of the best metal-semiconductor field effect transistors. And it decreases down to 0.3 dB at 8 GHz for an ambient temperature of -60 °C. An empirical noise model for the GFETs considering both temperature and gate voltage has been proposed and verified by the experimental results.

In conclusion, a way to characterise the temperature dependence of noise performance of the GFETs is discussed, which allows for further development of low-noise GFETs for high-frequency applications.

Keywords: graphene, GFET, noise characterisation, thermal experiments, minimum noise figure, F_{50} method, field effect transistors, microwave electronics

Acknowledgements

First, I would like to give my greatest gratitude to my supervisor Ms. Xinxin Yang who gave me a lot of assistance and instruction in this work and she also encouraged me whenever I had problems with it. She is always very patient to read the thesis and paper and give me advise for many times.

I would also like to thank Dr. Andrei Vorobiev who is always willing to discuss and give me suggestions helpfully. And I would like to thank Prof. Jan Stake who provides me with this great opportunity to working in the TML. And I also want to say thanks to Ms. Marlene Bonmann and Mr. Muhammad Asad for the help of the fabrication of the device. And I also want to thank Ms. Eunjung Cha for providing her device for measuring and comparing. And I would thank Prof. Serguei Cherednichenko for the advice and the help of the measurement equipment. And I want to show my respect to Dr. Michael Andersson who gives many useful advice and documents for the measurement.

Finally, I would like to thank my family and friends for supporting me all the time.

Junjie Li, Gothenburg, August 2019

Contents

List of Figures

List of Tables

List of Abbreviations

Al	aluminium
Al_2O_3	aluminium oxide
CMOS	complementary metal-oxide-semiconductor
CVD	chemical vapour deposition
DUT	device-under-test
ENR	excess noise ratio
FET	field effect transistor
GaAs	gallium arsenide
GFET	graphene field effect transistor
hBN	hexagonal boron nitride
HEMT	high electron mobility transistor
InP	indium phosphide
LNA	low noise amplifier
MESFET	metal-semiconductor field effect transistor
MOSFET	metal oxide semiconductor field effect transistor
SiC	silicon carbide
SiO_2	silicon oxide
SNR	signal-to-noise power ratio
RF	radio frequency
THz	terahertz

List of Notations

Γ_s	source reflection coefficient
Γ_L	load reflection coefficient
Γ_{opt}	source reflection coefficient for minimum noise
μ	carrier mobility
ω	angular frequency
a	lattice constant
B	noise bandwidth
C_{ds}	stray capacitance between electrodes
C_g	gate capacitance
C_{gd}	gate-drain capacitance
C_{gs}	gate-source capacitance
C_{pg}	gate pad capacitance
C_{pd}	drain pad capacitance
F	noise factor
F_{50}	noise figure with 50 Ω termination
F_{min}	minimum noise figure
f_T	transit frequency
f_{max}	maximum frequency of oscillation
G	gain
G_{av}	available gain
g_{ds}	drain conductance
g_m	transconductance
h_{21}	short circuit current gain
I_d	drain current
k_B	Boltzmann's constant
L	gate length
M	noise measure
n	charge carrier concentration
n_0	residual charge carrier concentration
N_a	component added noise power
N_c	cold-source noise power
N_h	hot-source noise power
N_i,N_o	input and output noise power
NF	noise figure
R_c	metal-graphene contact resistance
R_d	drain resistance
R_g	gate resistance

R_s	source resistance
R_n	noise resistance
r_{gs}	gate-source resistance
S_i,S_o	input and output signal power
T_a	ambient temperature
T_c	cold temperature of the noise source
T_d	equivalent drain temperature
T_g	equivalent gate temperature
T_h	hot temperature of the noise source
T_{min}	minimum noise temperature
T_0	standard temperature 290 k
U	unilateral power gain
v_{drift}	drift velocity
V_{ch}	channel potential
V_{dirac}	voltage at Dirac point
V_{ds}	drain voltage
V_{gs}	gate voltage
W	gate width
Y_{cor}	correlation admittance
Y_{opt}	optimum admittance

1
Introduction

High-frequencies electronics working at microwaves (0.3 - 100 GHz) and terahertz waves (loosely defined as 0.1 - 10 THz) have attracted a large number of interests because of their existing and potential applications. Nowadays, microwave electronics have been extensively used for wireless communication from mobile phones to satellites. Over the past few decades, the terahertz part of the electromagnetic spectrum has also been studied to a large extent. The larger bandwidth and lower energy of terahertz waves can make it be used in medicine and disease diagnostics [1], security inspection [2] and high-speed communication [3]. Most of these applications rely on the development of high-frequency field-effect transistors (FETs) and integrated circuits.

The FET is a three-terminal device where the current that flows through can be controlled by an electric field applied at the gate. The first FET was invented by William Shockley, John Bardeen and Walter Brattain in 1952 [4]. The traditional FETs are made of Si and GaAs which have been widely used as digital logic devices and radio-frequency devices. However, the operating frequency of traditional FETs is less than 50 GHz due to the limitation of the structure and material. There are two ways to increase the operating frequency of the FETs: either to improve the structure or introduce new material with better properties. The high electron mobility transistor (HEMT) invented by T. Mimura in 1979 utilises GaAs and AlGaAs heterostructer to form a two-dimensional electron gas channel [5]. And then $\mathrm{In_xGa_{1-x}As}$ was introduced to increase the mobility which shows a very high maximum frequency of oscillation f_{max} up to 1.2 THz [6].

However, for even higher frequencies, the new material with higher electron mobility such as the two-dimensional semi-metal material, graphene, was introduced by Novoselov *et.al* in 2004 [7]. Since then it has raised a lot of interest in fundamental researches as well as applications. Graphene has only one layer of carbon in a hexagonal honeycomb lattice with a carbon-carbon bond length of 1.42 Å and the lattice constant of a = 2.476 Å. Unlike the conventional semiconductor material which has a bandgap between the valence band and conduction band, there are six points in momentum space of graphene that has no bandgap. Around these points, the dispersion relation of graphene is approximately linear and these points are named Dirac point. The unique structure of graphene gives it a remarkable electron mobility at room temperature, more than 2×10^5 $\mathrm{cm^2/Vs}$ with a suspended monolayer in vacuum [8]. These properties make it a very suitable channel material for high-frequency FETs. The first top-gated graphene field-effect transistor (GFET) was investigated in 2007 [9]. Also, the atomic thickness of graphene allows GFETs to be scaled to shorter channel lengths and higher speeds without encountering the adverse short-channel effects [10]. It is also possible to combine graphene with plastic substrates to make a flexible device which is essential for the future of internet of things (IoT) [11]. The transit frequency f_T and the maximum frequency of oscillation f_{max} derived from the short-circuit current gain, $|h_{21}|$=1, and the Mason gain, U=1 [12,13] of the state-of-the-art GFETs are summarised and compared with other high frequency FETs in Fig.1.1 [14,15]. The f_T of GFETs is comparable with HEMTs, but the f_{max} is much lower due to the absence of bandgap.

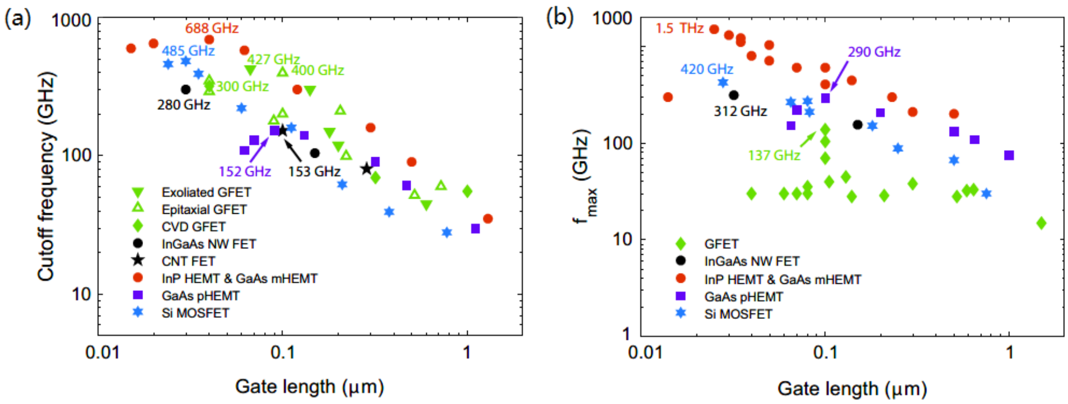

Figure 1.1: State-of-the-art intrinsic (a) f_T and (b) f_{max} for HEMTs, Si CMOSs, CNT and NW FETs against reported GFETs [14,15].

In addition, to enhance operating frequencies, improving the noise performance of GFETs is another challenging task. For high-frequency operation, minimum noise figure (F_{min}), as important as f_T and f_{max}, has been reported by a few papers. The first GFET amplifier with power gain was reported in 2012 which has an extrinsic minimum noise figure (F_{min}) of 3.3 dB at 1 GHz [16]. A F_{min} of 2.4–4.9 dB was obtained in 2–8 GHz for the extrinsic chemical vapour deposition (CVD) graphene FET on silicon substrate [17]. The quasi-freestanding bilayer graphene grown on an SiC (0001) substrate with a F_{min} of 0.8-3.6 dB in 10-26 GHz [18] and the flexible graphene microwave transistors with a F_{min} of 1.34 dB at 5.5 GHz [19] were reported. The F_{min} of the latest GFETs is compared with other high-frequency FETs in Fig.1.2. It shows that the noise of the GFETs [18] is similar to COMS [20] and MESFET [21], but higher than HEMTs [22, 23]. However, the temperature influence of the noise for GFETs hasn't been discussed yet. Temperature usually plays an important role in the noise performance of transistors and the traditional FETs have been reported that they can have lower noise when operated at a lower temperature. This thesis will discuss a way to measure the F_{min} of GFETs and find out its temperature dependence.

1.1 Thesis outline

In this thesis, the noise characterisation of GFETs is performed with different temperature and bias conditions. Chapter 2 introduces the noise theory and discusses two different high-frequency noise characterisation techniques and two calculation

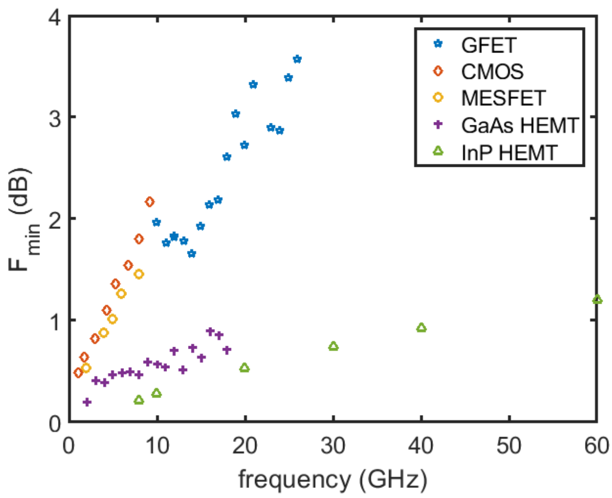

Figure 1.2: F_{min} for HEMTs, Si CMOS, MESFET and against reported intrinsic GFETs [18,20,21,22,23].

methods of high-frequency noise parameters. Chapter 3 shows the fabrication process, experimental results and noise modelling of the GFETs. Chapter 4 concludes the work results and depicts the possible future work.

2
Theoretical background

Amplifiers are crucial building blocks of any communication system and the block diagram of a microwave amplifier is shown in Fig.2.1 [24]. At high frequencies, the thermal noise will affect the output signal. Therefore, it is necessary to study the noise theory and develop low-noise amplifiers. In this chapter, two different high-frequency noise characterisation techniques, i.e., the Y-factor and cold-source methods, and two calculation methods of high-frequency noise parameters, i.e., the source-pull and 50 Ω impedance termination methods, will be analysed and discussed.

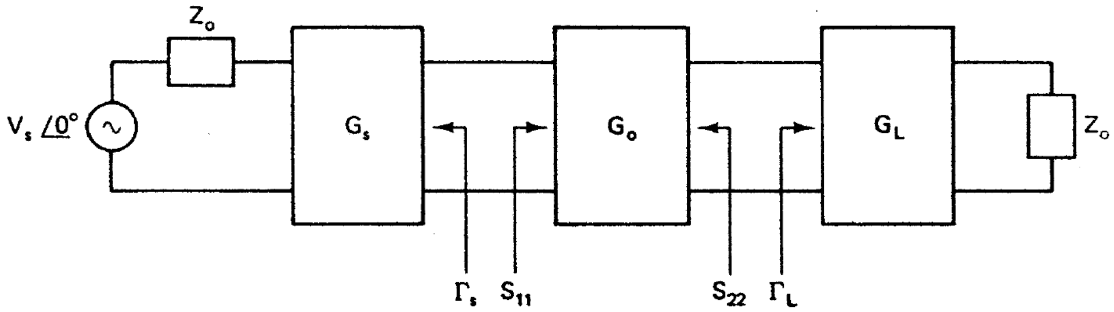

Figure 2.1: A block diagram of a microwave amplifier [24].

2.1 Noise theory

2.1.1 Noise

The noise in semiconductor devices is referred to the spontaneous fluctuation in current or voltage which is considered as an undesired effect. The most important four kinds of noise in GFETs are

- Thermal or Johnson noise, which originates from the kinetic energy of charge carriers inside an electrical conductor at equilibrium [25, 26].
- Shot noise, which is caused by the quantized and random nature of the current flow [27].
- Generation-recombination (G-R) noise, which is due to the fluctuations of free carriers number associated with random transitions of charge carriers between states in different energy bands [28].
- Flicker or $1/f$ noise, which has a $1/f$ power spectral density and it is a low-frequency phenomenon [29].

The G-R noise is lower than gigahertz [28] and the shot noise and flicker noise become important only when FETs have a large gate leakage current [29]. Therefore, this thesis will only investigate the thermal noise for high-frequency devices.

2.1.2 Noise parameters

To characterise the noise for high-frequency FETs, a figure of merit is required to describe the performance of it.

The highest output signal-to-noise power ratio (SNR) of a system equals to the input SNR when all the components in the system is noiseless. But usually, the components which refers to FETs here have their own noise that decreases the output SNR. So the ratio of the signal-to-noise power ratio at the input to the signal-to-noise power ratio at the output, defined as the noise factor (F), can describe the noise performance of a FET [30]:

$$F = \frac{S_i/N_i}{S_o/N_o}, \tag{2.1}$$

where S_i and S_o are the input and output signal power, N_i and N_o are the input and output noise power, respectively.

F is a figure-of-merit that describes the degradation of SNR due to the noise caused by the components in a signal chain. Take the amplifier as an example, if the amplifier is noiseless, then the output signal is simply the input multiplied by the amplifier gain. But realistically, the amplifier also has noise and the output signal is larger than the input signal multiplied by the gain. So F can be expressed as

$$F = \frac{S_i/N_i}{GS_i/\left(N_a + GN_i\right)} = \frac{N_a + GN_i}{GN_i}, \tag{2.2}$$

where N_a is the noise added by the amplifier, G is the gain of the amplifier.A system amplifies signal and noise at the same time which does not change the SNR. Therefore, SNR is only dependent on the temperature of the noise source, which means the F should not be related to the gain.

F is a property of a device-under-test (DUT) which is not dependent on the input signal. The F of a DUT is influenced by the impedance mismatch between the noise source and DUT, and the impedance match between DUT and the measuring instrument. Therefore, a special tuner is needed to provide a certain source reflection coefficient to make a perfectly matched system. The F depending on source impedance presented by the tuner is described by as

$$F = F_{min} + \frac{4R_n}{Z_c}\frac{|\Gamma_{opt} - \Gamma_s|^2}{|1+\Gamma_{opt}|^2\left(1 - |\Gamma_s|^2\right)}, \tag{2.3}$$

where F_{min} is the minimum noise factor and R_n is the noise resistance. Γ is the source reflection coefficient. Only when $\Gamma_s = \Gamma_{\text{opt}}$, the F of the system equals F_{min}. F_{min}, R_n and Γ_{opt} are usually frequency dependent.

The DUT cannot be measured individually. Usually, it is measured in a system. To find the F of the component that is interested, the F of the overall system and the gain of other components are needed. Then the F of the device can be calculated from the overall noise figure:

$$F_{sys} = F_1 + \frac{F_2 - 1}{G_1}. \tag{2.4}$$

The noise measure (M) is another important parameter for a system when considering cascaded two-ports [31] and it is defined as

$$M = \frac{F - 1}{1 - \frac{1}{G_a}}, \tag{2.5}$$

where G_a is the available power gain and the M is a function of source admittance.

For high-frequency FETs, thermal noise is the most important noise source. Because the thermal noise of an electric system usually comes from the vibration of carriers, including electrons and holes. And the vibrations spectral is nearly uniform over RF and microwave frequencies, which is the signal spectral that is interested. So it will contribute to the signal-to-noise power ratio (SNR). The noise power of a thermal source at temperature T is $N = k_B T B$, where k_B is Boltzmann's constant (1.38×10^{-23} J/ K) , and B is the system's noise bandwidth. The IRE (forerunner of the IEEE) adopted 290 K as the standard temperature T_0 for thermal source at the input. Then the F becomes

$$F = \frac{T_a}{T_0} + 1. \tag{2.6}$$

where T_a is the noise temperature of the DUT.

F in Eq. (2.1-2.6) is often called noise factor or sometimes noise figure in linear terms. Noise figure usually is F expressed in log scale:

$$NF = 10 \log_{10} F. \tag{2.7}$$

2.1.3 Pospieszalski's noise model

In high-frequency FETs, the thermal noise comes from the resistive parts of the channel, parasitic resistances and high-field diffusion noise from the velocity saturated part of the channel [32]. The intrinsic FET can be considered as a linear two-port system as the equivalent circuit using different matrix representations as in Fig.2.2 [33, 34]. Fig.2.2a shows an equivalent circuit with two noise current sources i_1 and i_2 with an inner infinite impedance represented by admittance matrix (Y). It can also present all the internal noise sources only at the input side by a noise current source i and a noise voltage source e represented by chain matrix (ABCD) as shown in Fig.2.2b.

In the equivalent circuit of GFETs, the noise can be expressed as drain and gate current sources, i_d and i_g. In Pospieszalski's noise model, the resistive elements of the intrinsic circuit are assigned to the unrelated equivalent gate and drain temperature T_g and T_d:

$$\overline{i_g^2} = 4 k_B \Delta f T_g / r_{gs}, \tag{2.8}$$

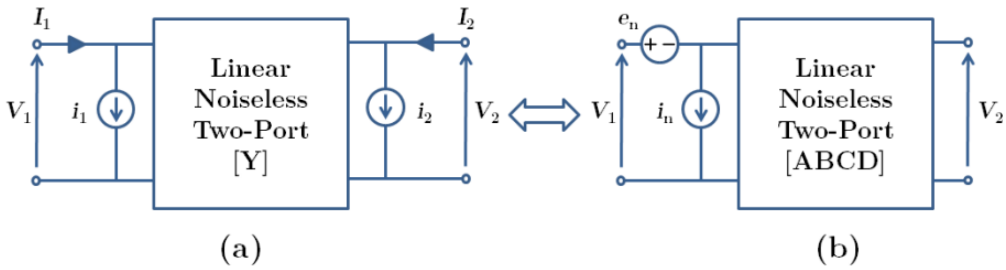

Figure 2.2: (a) Equivalent circuit with the outside noise current sources i_1 and i_2 respectively. (b) Equivalent circuit with noise voltage source e and noise current source i at the input [33,34].

$$\overline{i_d^2} = 4k_B \Delta f T_d g_{ds}, \tag{2.9}$$

where Δf is the incremental bandwidth [35]. The r_{gs} is the gate-source resistance and g_{ds} is the drain conductance which are shown in the intrinsic equivalent circuit of FETs in Fig.2.3 [36].

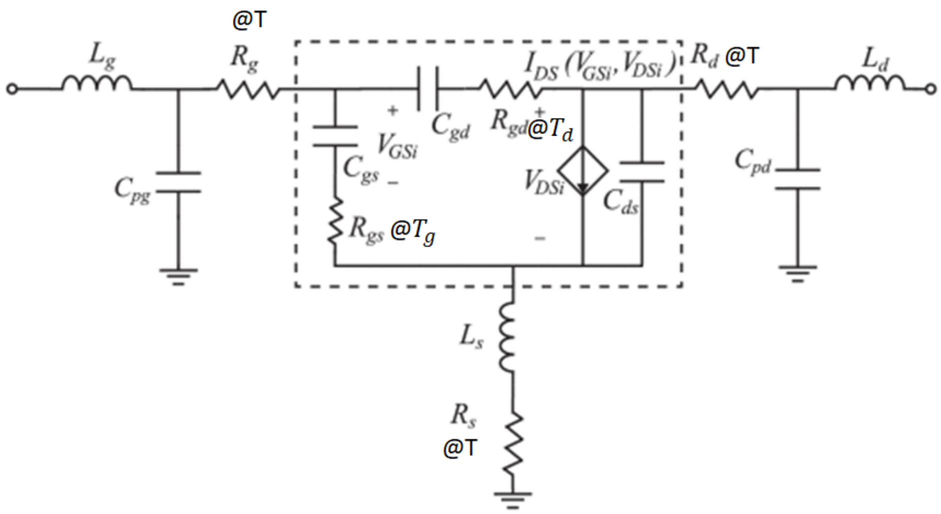

Figure 2.3: Equivalent circuit and the noise model of GFETs [36].

And the minimal noise temperature can be expressed by T_g and T_d:

$$R_{opt} = \sqrt{\left(\frac{f_T}{f}\right)^2 \frac{r_{gs}}{g_{ds}} \frac{T_g}{T_d} + r_{gs}^2}, \tag{2.10}$$

$$g_n = \left(\frac{f}{f_T}\right)^2 \frac{g_{ds} T_d}{T_0}, \tag{2.11}$$

$$R_n = \frac{T_g}{T_0} r_{gs} + \frac{T_d}{T_0} \frac{g_{ds}}{g_m^2} \left(1 + \omega^2 C_{gs}^2 r_{gs}^2\right), \tag{2.12}$$

$$T_{\min} = 2\frac{f}{f_T}\sqrt{g_{ds}r_{gs}T_gT_d + \left(\frac{f}{f_T}\right)^2 r_{gs}^2 g_{ds}^2 T_d^2} + 2\left(\frac{f}{f_T}\right)^2 r_{gs}g_{ds}T_d, \tag{2.13}$$

where g_m is the transconductance, ω is the frequency, C_{gs} is gate-source capacitance and f_T is cut-off frequency. The relationship between F_{min} and T_{min} is

$$F_{min} = \frac{T_{min}}{T_0} + 1. \tag{2.14}$$

2.2 High-frequency noise characterization techniques

2.2.1 Y-factor method

The most basic method for noise measurements is the Y-factor method, which is also called the hot-cold method. The output noise power of a device is linear with temperature as shown in Fig.2.4 [37].

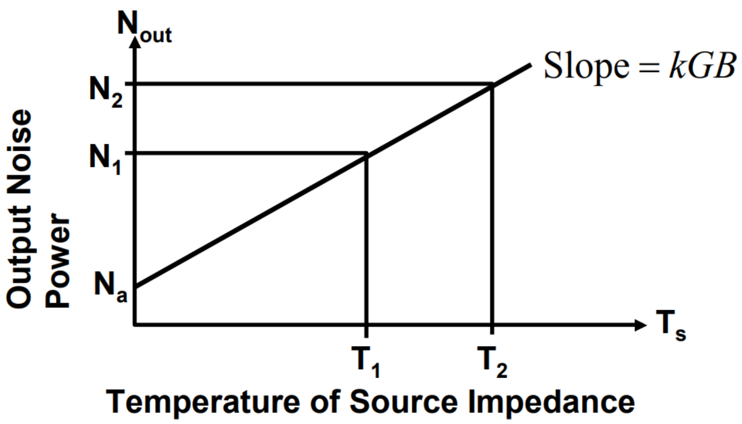

Figure 2.4: The output noise power versus source temperature of linear, two-port devices [30].

According to this relationship, the gain and N_a of a device can be found from the slop and a reference point. And the F can be calculated from N_a by Eq.2.6. Y-factor is defined as the ratio of the noise power at low temperature N_c and noise power at high temperature N_h, which can be measured when the noise source is off and on:

$$Y = \frac{N_h}{N_c}. \tag{2.15}$$

Then the F can be expressed by Y-factor as

$$F = \frac{\left(\frac{T_h}{T_0} - 1\right) - Y\left(\frac{T_c}{T_0} - 1\right)}{Y - 1}. \tag{2.16}$$

Assuming that the cold temperature T_c is equal to the reference temperature $T_0 = 290\text{K}$. And the excess noise ratio (ENR) of a noise source is defined by

$$ENR = \frac{(T_h - T_0)}{T_0}, \tag{2.17}$$

which is usually given by the manufacturer. Now the F can be obtained from only a Y factor:

$$F_Y = \frac{ENR}{Y-1}. \tag{2.18}$$

2.2.2 Cold-source method

The Y-factor method is convenient, but it is difficult to measure the low gain or lossy devices since the difference in noise between the hot and cold states of the noise source is reduced to a very small amount by the attenuator. Another method called the cold-source method is valid to measure the noise figure of an attenuator or mismatched devices [37]. Because the cold-source technique computes the noise figure only from a single noise measurement N_c which means that a better termination can be used at room temperature. The F calculated by the cold-source method is expressed by

$$F_{CS1} = \frac{N_c}{T_0 k_B B G_{rec} G_{av}\left(\Gamma_{sc}\right)}. \tag{2.19}$$

where kBG_{rec} is the gain-bandwidth product of the receiver, $G_{a\nu}\left(\Gamma_{sc}\right)$ is the available gain of the DUT. The room temperature is assumed to be equal to the reference temperature T_0 again [38].

In order to obtain an absolute noise power, the receiver power calibration is needed which includes the use of a calibrated hot noise source during the calibration step. And after considering the second stage correction, the cold-source noise figure becomes

$$F_{CS2} = \frac{N_c - N_{c\_rec}}{T_0 k_B B G_{rec} G_{av}\left(\Gamma_{sc}\right) MM\left(\Gamma_{ou}\right)} + \frac{1}{G_{av}\left(\Gamma_{sc}\right)}. \tag{2.20}$$

where MM is a mismatch term between the noise source and can be calculated from S-parameter as

$$MM(\Gamma) = \frac{1 - |\Gamma|^2}{\left|1 - s_{11\_rec}\Gamma\right|^2}. \tag{2.21}$$

And the factor kBG_{rec} is given by

$$k_B B G_{rec} = \frac{N_{h\_rec} - N_{c\_rec}}{T_h - T_0}. \tag{2.22}$$

where N_{c_rec} and N_{h_rec} is the output noise power measured with only the receiver after the noise source at cold and hot temperature respectively. T_h is the hot temperature of the noise source calculated from its ENR.

2.3 F_{min} calculation methods

Generally, it is not possible to obtain both minimum noise and maximum gain for an amplifier. The minimum noise figure is a trade-off between noise figure and gain. Here we present two different ways to calculate the minimum noise figure from the measured noise figure.

2.3.1 Source-pull method

According to Eq.2.3, F varies with different source reflection coefficient Γ_s and F_{min} occurs when $\Gamma_s = \Gamma_{opt}$. The source-pull method is a way to vary the source impedance in front of a DUT while measuring the noise performance of the DUT. There are four unknown parameters in the equations. Therefore, at least four measured noise figures are needed for least-square fitting in order to find out the F_{min}. In most cases, a tuner is used to provide different source reflection coefficients.

If x and y are set to be

$$x = \frac{|\Gamma_S - \Gamma_{opt}|^2}{\left(1 - |\Gamma_S|^2\right)|1 + \Gamma_{opt}|^2}, \tag{2.23}$$

$$y = F = F_{\min} + \frac{4R_n}{Z_0}x, \tag{2.24}$$

then the F is linear with x. So by least-square fitting with each impedance and noise figure, the F_{min} can be found.

F_{min} can also be found from the circles of constant noise figure. The noise figure parameter N is defined as [39]

$$N = \frac{|\Gamma_S - \Gamma_{opt}|^2}{1 - |\Gamma_S|^2} = \frac{F - F_{min}}{4R_N/Z_0}\,|1 + \Gamma_{opt}|^2\,. \tag{2.25}$$

A fixed noise figure can be shown as a circle in the Smith plane [31]. The centre and radius of the circle of constant noise figure can be calculated as

$$C_F = \frac{\Gamma_{opt}}{N+1}, \tag{2.26}$$

$$R_F = \frac{\sqrt{N\left(N + 1 - |\Gamma_{opt}|^2\right)}}{N+1}. \tag{2.27}$$

The circles for all impedance can be plotted on one Smith plane. And the point of the Γ_{opt} and the F_{min} can be found when all the circles shrinks to a point as shown on the Fig.2.5.

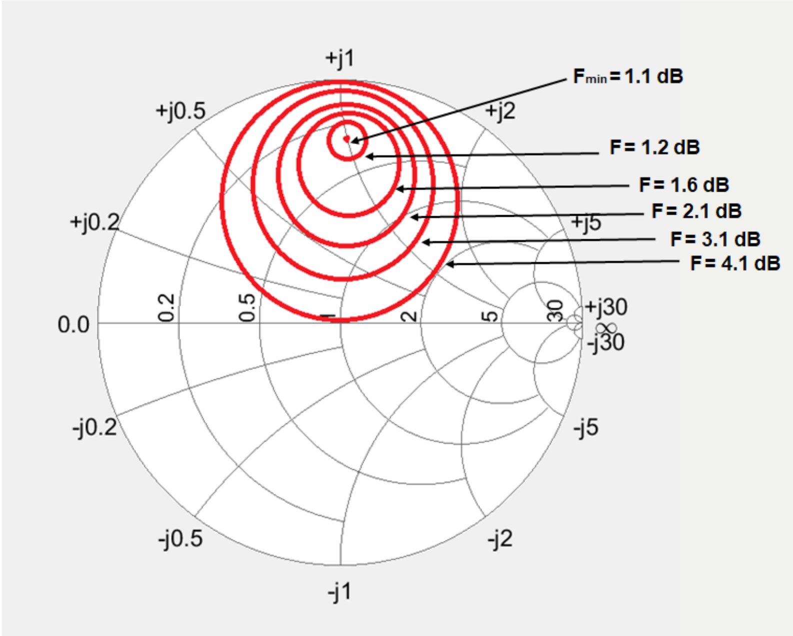

Figure 2.5: Circles of a series of constant noise figure [39].

2.3.2 50 Ω termination method

This method allows for direct extraction of the $F_{\min}$ from a single noise figure measurement with a simple 50 Ω noise source [40]. The Eq.2.3 can be also expressed as

$$F = F_{\min} + N\frac{|Z_s - Z_{opt}|^2}{R_s R_{opt}}, \tag{2.28}$$

$$T = T_{min} + T_0 N \frac{4\left|\Gamma_{\mathrm{s}} - \Gamma_{opt}\right|^2}{\left(1 - |\Gamma_s|^2\right)\left(1 - |\Gamma_{opt}|^2\right)}. \tag{2.29}$$

And if the noise source is 50 Ω generator impedance ($Y_g = G_0 = 20$ mS), the noise figure F_{50} can be deduced from Eq.2.3 and becomes [41]

$$F_{50} = 1 + R_n \cdot G_o + \frac{R_n}{G_o} \cdot \left(2 \cdot G_o \cdot G_{cor} + |Y_{opt}|^2\right). \tag{2.30}$$

where Y_{opt} is optimum admittance and G_{cor} is the real part of the correlation admittance Y_{cor}. R_n is mostly frequency independent according to the previous experiments. So F_{50} is also linear with ω^2 and when $\omega = 0$, the value of F_{50} is

$$F_{50} = 1 + R_n \cdot G_o, \quad w = 0. \tag{2.31}$$

Thus R_n can be easily deduced from the F_{50} extrapolation at $\omega = 0$ [41]. Then, according to Pospieszalski's noise model,the R_n can also be expressed as

$$R_n = \frac{T_g}{T_0} r_{gs} + \frac{T_d}{T_0}\frac{g_{ds}}{g_m^2}\left(1 + \omega^2 C_{gs}^2 r_{gs}^2\right). \tag{2.32}$$

Assume that the gate temperature T_g is simply equal to the ambient temperature T_a [40, 42]. And the T_d can be derived to be

$$T_d = \frac{R_n - R_i}{1 + \omega^2 C_{gs}^2 R_i^2} \frac{T_0 g_m^2}{g_{ds}}, \quad T_g = T_0, \quad r_{gs} = R_i. \tag{2.33}$$

All the intrinsic parameters can be extracted from the small-signal equivalent circuit of GFETs shown in Fig.2.3. Together with its S-parameters, the parameters can be obtained through the following expressions [43, 44]:

$$C_{gd} = -\frac{\mathrm{lm}\left(Y_{12}\right)}{\omega}, \tag{2.34}$$

$$C_{gs} = \frac{\mathrm{Im}\left(Y_{11}\right) - \omega C_{gd}}{\omega} \left(1 + \frac{\left(\mathrm{Re}\left(Y_{11}\right)\right)^2}{\left(\mathrm{Im}\left(Y_{11}\right) - \omega C_{ed}\right)^2}\right), \tag{2.35}$$

$$R_i = \frac{\mathrm{Re}\left(Y_{11}\right)}{\left(\mathrm{Im}\left(Y_{11}\right) - \omega C_{gd}\right)^2 + \left(\mathrm{Re}\left(Y_{11}\right)\right)^2}, \tag{2.36}$$

$$g_m = \sqrt{\left(\left(\mathrm{Re}\left(Y_{21}\right)\right)^2 + \left(\mathrm{Im}\left(Y_{21}\right) + \omega C_{gd}\right)^2\right)\left(1 + \omega^2 C_{gs}^2 R_i^2\right)}, \tag{2.37}$$

$$\tau = \frac{1}{\omega} \arcsin\left(\frac{-\omega C_{gd} - \mathrm{Im}\left(Y_{21}\right) - \omega C_{gs} R_i \,\mathrm{Re}\left(Y_{21}\right)}{g_m}\right), \tag{2.38}$$

$$C_{ds} = \frac{\mathrm{Im}\left(Y_{22}\right) - \omega C_{gd}}{\omega}, \tag{2.39}$$

$$g_{ds} = \mathrm{Re}\left(Y_{22}.\right) \tag{2.40}$$

The T_d versus frequency can be obtained by solving Eq.2.31, Eq.2.32 and Eq.2.33 together. And the corresponding R_{opt} and T_{min} can be derived to be

$$R_{opt} = \left[r_{gs}^2 + \left(\frac{g_m}{\omega c_{gs}}\right)^2 \frac{T_g r_{gs}}{T_d g_{ds}}\right]^{\frac{1}{2}}, \quad x_{opt} = \frac{1}{\omega c_{gs}}, \tag{2.41}$$

$$T_{\min} = 2\left(\frac{\omega c_{gs}}{g_m}\right)^2 \left(T_d g_{ds}\right)\left(r_{gs} + R_{opt}\right). \tag{2.42}$$

Then the F_{min} can be calculated by using Eq.2.14.

2.3.3 Comparison and analysis

The source-pull method is easy on the calculation, but it is usually time-consuming. And the error correction of the source-pull method is complex which requires specialised measurement systems. In addition, it is difficult to find suitable measurement points (source impedance) to obtain valid data for fitting. Compared with the source-pull method, the 50 Ω method only needs one measured noise figure and the measurement system is easy to be integrated into fully automated RF s-parameter measurement systems [40]. The result of it has a good agreement with the conventional source-pull method for the MESFET and HEMT as shown in Fig.2.6 [41].

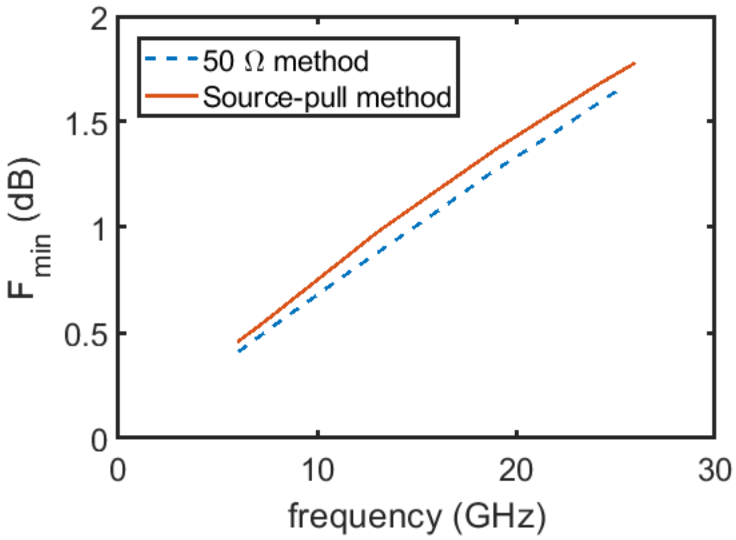

Figure 2.6: Comparison of the measured four noise parameters versus frequency. Solid line: conventional technique by using source-pull. Dashed line: 50Ω termination method [41].

3

Fabrication and characterisation of GFETs

In this chapter, the experimental process and noise results of the GFETs are illustrated. Device fabrication, dc characterisation, S-parameters and noise figure measured at different ambient temperature and bias conditions are shown. The noise measurements are carried out in a noise parameter characterisation setup using the cold-source method with 50 Ω termination. An empirical noise model for the GFET on temperature and gate bias dependence is proposed at the end of this chapter which is necessary for the future design of graphene low-noise amplifiers.

3.1 GFET design and fabrication

There are three ways to obtain high-quality graphene. One is mechanical exfoliation [45], and the others are chemical vapour deposition (CVD) [46] and thermal decomposition of SiC [47, 48]. Exfoliation is mostly used in laboratories for higher quality and CVD suits industry for wafer-scale graphene. The GFETs measured in this thesis are made of CVD graphene and the side view and layout of the GFETs are shown in Fig.3.1.

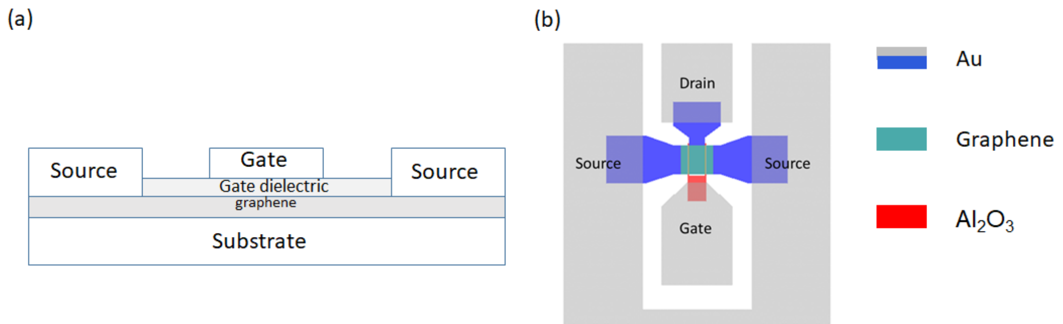

Figure 3.1: (a) Side view of the GFET. (b) Layout of the GFET.

To fabricate these graphene transistors, following processing techniques can be applied [17, 49]:

- Graphene transfer: The target transfer substrates is Si with 90 nm SiO_2.
- Graphene mesa: 1 nm of Al is evaporated on top of the graphene and oxidised in the air twice to form a protective layer. The pattern of the graphene channel

is defined by e-beam lithography. Other parts of graphene are etched by oxygen plasma.

- Ohmic contact: The electrodes of source and drain are patterned by E-beam lithography and lift-off process.
- Gate dielectric: Al_2O_3 dielectric is formed by evaporation 1 nm Al and natural oxidation in the air for six times.
- Gate contact: E-beam lithography is applied again to form the gate contact pattern and evaporate 10 nm Ti or 200 nm Au on the dielectric.
- Pad contacts: The contact pads are formed after a final e-beam lithography and Ti or Au evaporation.

Fig.3.2 displays the SEM image of the GFET [50] that is fabricated from the above process and measured in the following experiments. The GFET has a gate of $0.75 \times 15\ \mu\text{m}^2$.

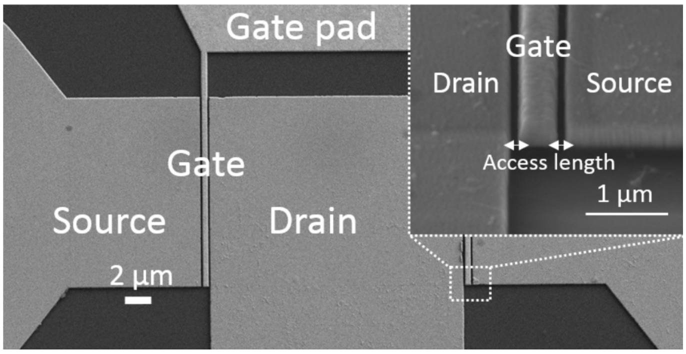

Figure 3.2: SEM image of a two-finger GFET with gate length $L_g = 0.75\ \mu$m and gate width $W_g = 2 \times 15\ \mu$m. The inset shows a 70° tilted view of the gate area [49].

3.2 DC characteristics

Fig.3.3a shows the drain current versus gate voltage at different temperatures for device A which has a $0.75 \times 15\ \mu\text{m}^2$ gate. The Dirac point of device A is around 0.1 V. The transfer curve of device A does not change too much under different temperatures. The shift of the Dirac point is within 0.1 V. However, the Dirac point of many other devices will shift a lot when temperature changes, like device B (with $0.75 \times 15\ \mu\text{m}^2$ gate) shown in Fig.3.3b. In order to simplify the characterisation and modelling, we will focus on device A first. In this case, the effect of the change of the Dirac point won't be considered in the later discussion.

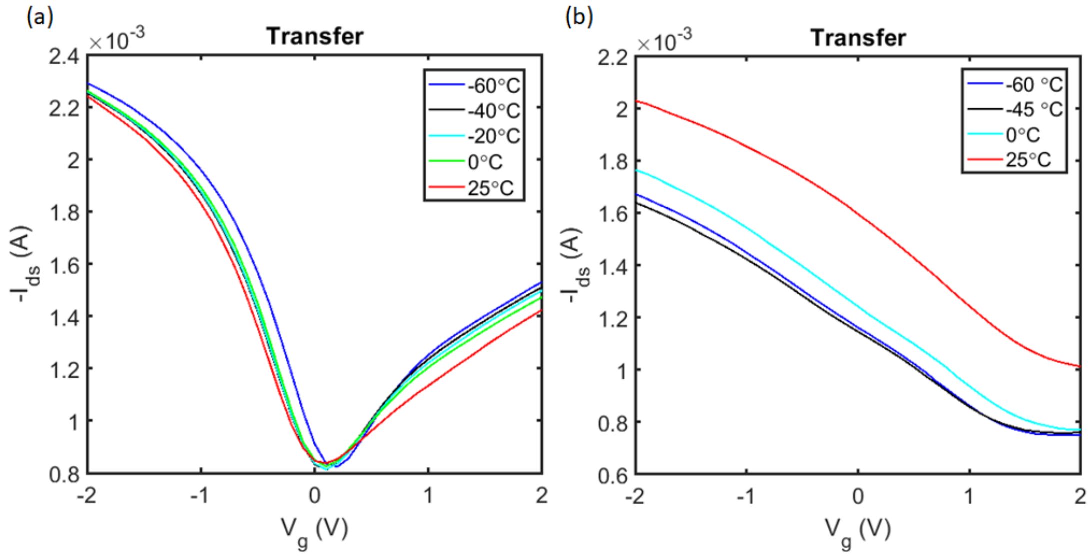

Figure 3.3: Transfer curve at drain voltage of 0.1 V and temperatures ranging from -60 °C to 25 °C for (a) device A and (b) device B.

By fitting the measured data of a transfer curve using Eq.3.1, Eq.3.2 and Eq.3.3, the relevant parameters can be extracted, such as the carrier concentration n_0, the mobility μ and the contact resistance R_{contact} [51]. For device A as shown on Fig.3.4, the n_0 is around 11.9×10^{11} cm^{-2}, the μ is around 3000 cm^2/Vs and the R_{contact} is around 30 Ω.

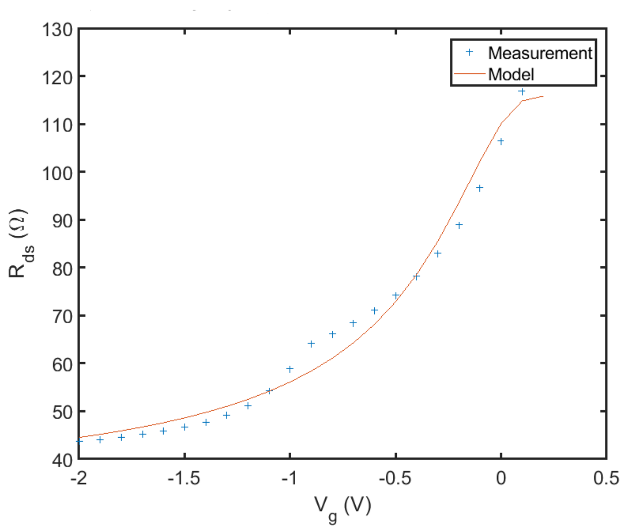

Figure 3.4: Fitting of the transfer curve of device A at 25 °C .

$$n_{\text{ total}} = \sqrt{n_0^2 + n\,[V_{TG}]^*}, \tag{3.1}$$

$$V_{TG} - V_{TG,\text{Dirac}} = \frac{e}{C_{ox}}n + \frac{\hbar v_F \sqrt{\pi \cdot n}}{e}, \tag{3.2}$$

$$R_{\text{total}} = R_{\text{contact}} + R_{\text{channel}} = R_{\text{contact}} + \frac{N_{sq}}{n_{\text{ total}}\, e\mu} = R_{\text{contact}} + \frac{N_{sq}}{\sqrt{n_0^2 + n\,[V_{TG}^*]^2}\, e\mu}. \quad (3.3)$$

For the output curve, we can see from Fig.3.5a that at -60 °C it has a higher current than that of 25 °C which is the same as expectation. This is mainly because of the decrease in the contact resistance at lower temperature. But if it is cooled down to cryogenic temperature as shown in Fig.3.5b, the drain current at 4k is even lower than that of 25 °C. This phenomenon may come from the change of other parameters at a very low temperature.

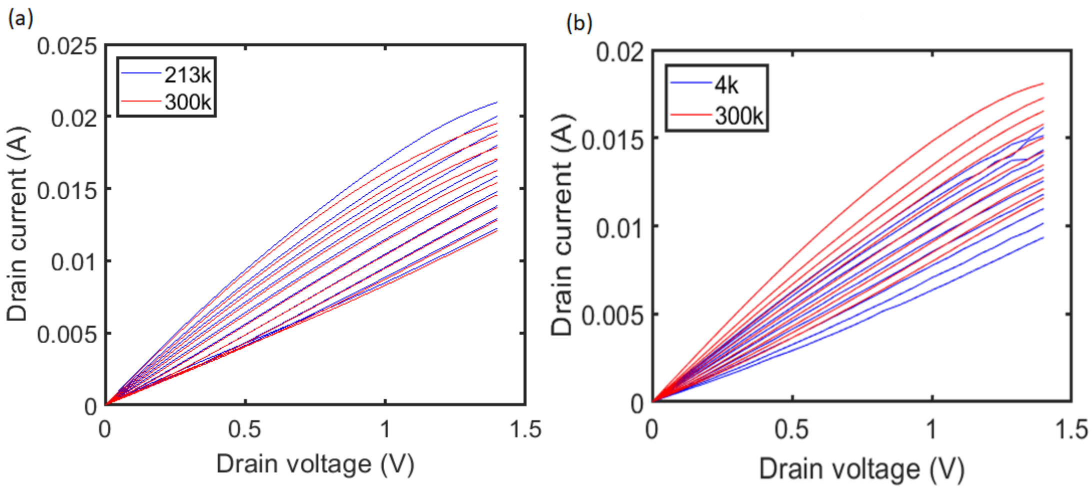

Figure 3.5: Output curve of device A at gate voltage from -1.2 V to 0.6 V in steps of 0.2 V (a) at 213 K and 300 K, respectively, and (b) at 4 K and 300 K, respectively.

3.3 S-parameters

The S-parameters are important for the extraction of the F_{min} according to the previous chapter. Therefore it is necessary to check how the S-parameters change with temperatures. Fig.3.6 shows the S_{11}, S_{12}, S_{21}, and S_{22}, of device A with drain voltage of -1.2 V and gate voltage of -0.7 V at five different temperatures. It is obvious that S_{21}, the complex linear gain, is affected most by the temperature.

The intrinsic parameters extracted from the S-parameters in the frequency range of 2 - 18 GHz at 298 k and 213 K are shown in Table.3.1 [43, 44]. Fig.3.7 shows the intrinsic transconductance (g_{mi}) at different ambient temperatures. Due to the short gate length, g_{mi} of the device is proportional to the number of carriers and their saturation velocity in the channel. Here it shows an approximately linear decrease with temperature which means the velocity saturation and the carrier density also have some dependence on temperature.

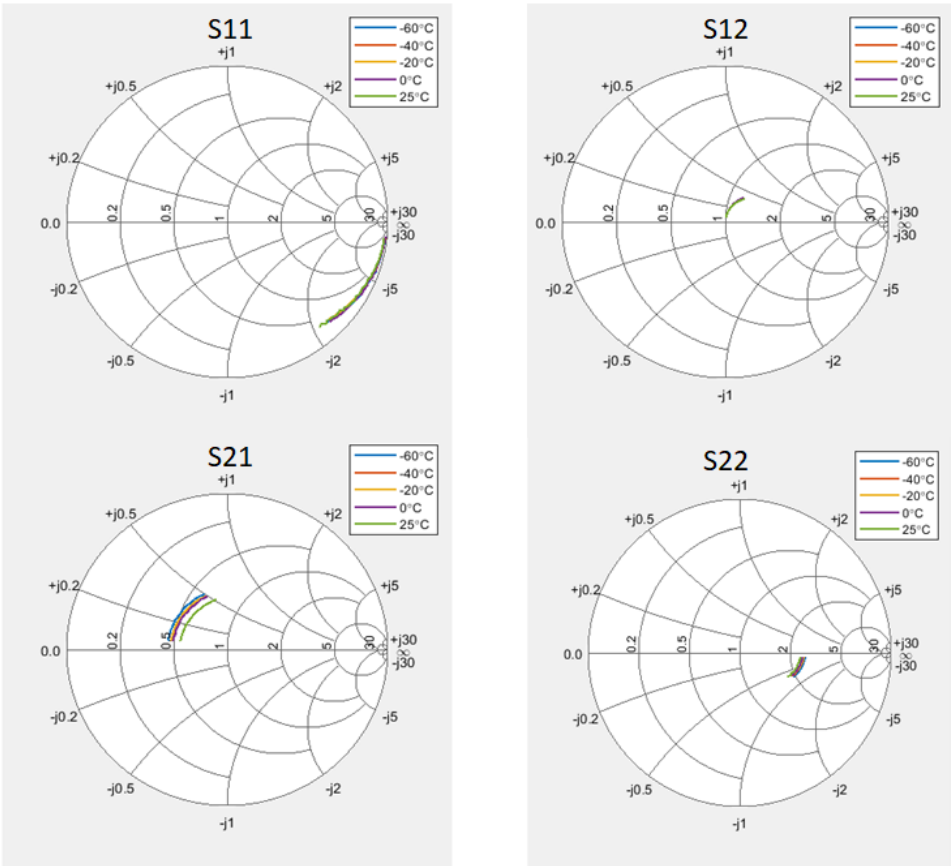

Figure 3.6: S-parameters of device A at V_g = -0.7 V V_d = -1.2 V at -60, -40, -20, 0 and 25 °C respectively.

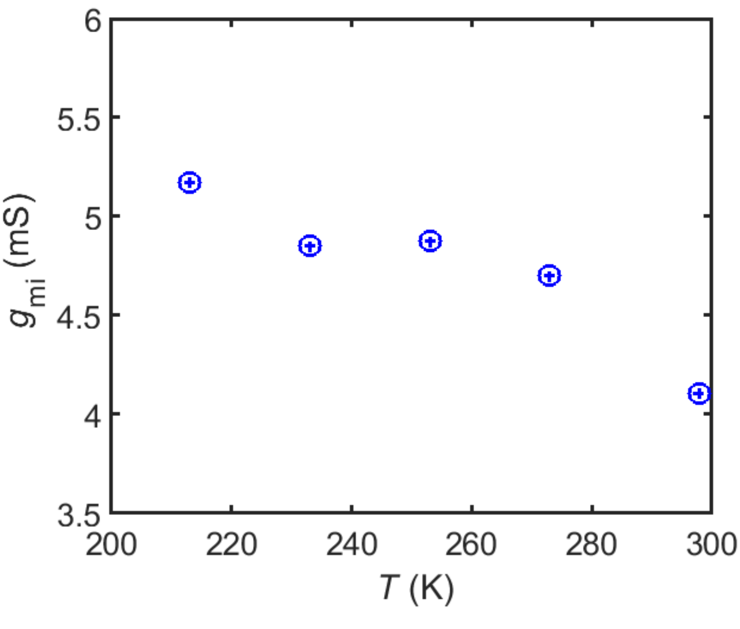

Figure 3.7: The intrinsic transconductance at V_g = -0.7 V, V_d = 1.2 V at different temperatures.

Table 3.1: De-embedded parameters for the GFET at V_{gs} = -0.7 V, V_{ds} = -1.2 V and ambient temperature of 213 K and 298 K.

T (K)	C_{gs} (fF)	C_{gd} (fF)	C_{ds} (fF)	g_{ds} (mS)	g_{mi} (mS)	τ (ps)	R_i (Ω)
298	27	26	20	7.7	4.1	0.10	3.4
213	25	25	17	6.8	5.1	0.13	4.8

3.4 Noise characterisation

3.4.1 Measurement setups

The source-pull measurement setup and schematic are shown in Fig.3.8 and Fig.3.9. The dc curves are measured by the source meter Keithley 2604B. The S-parameters in the frequency range of 2-18 GHz are measured by the network analyser Agilent N5230A. The different source reflection coefficients are provided by an electronic mismatch source tuner A433067 (2-26.5 GHz) which is connected to the GFET through a bias tee. The source tuner is integrated with a switch that can be controlled by NP5 Wafer Probe Test Set (control box) to switch between the VNA and NFA. The F is measured by Agilent N8975A noise figure analyser (NFA) with Keysight N4002A SNS Series Noise Source (10 MHz-26.5 GHz) and the NFA can also control the cold and hot state of the noise source. All the frequency points were measured for more than four tuner states. In each state, the source tuner presents a different source impedance to the GFET at each frequency. The testing and reading of VNA, NFA and the control box are controlled via GPIB.

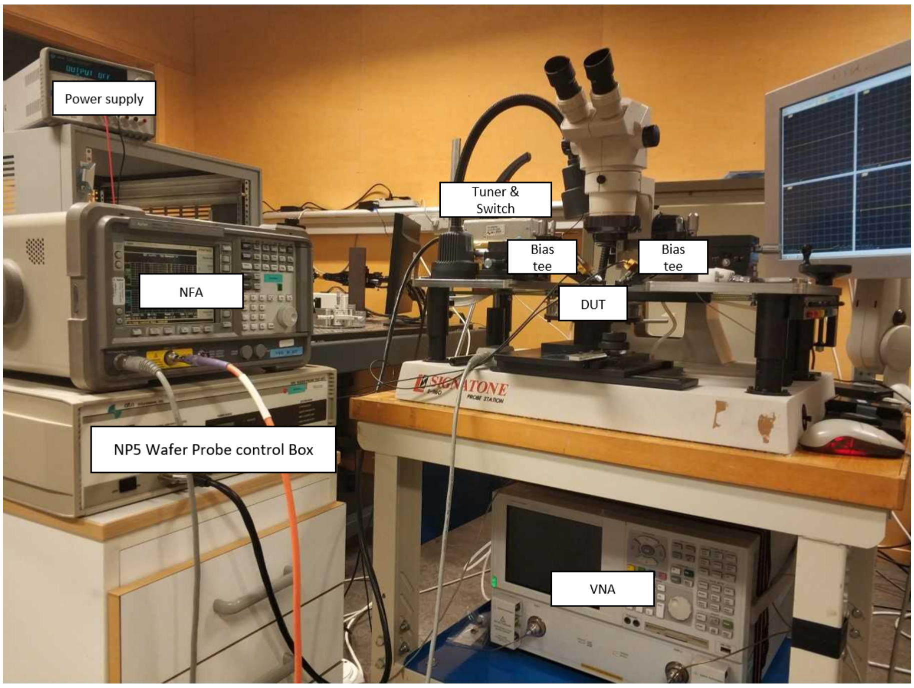

Figure 3.8: The source-pull noise measurement setup.

The 50 Ω termination method doesn't need the tuner and the setup schematic is shown in Fig.3.10. The dc curves are also measured by the source meter Keithley 2604B. The S-parameters in the frequency range of 2-18 GHz are measured by the network analyser (VNA) Agilent E8361A. And the F_{50} of the GFET was measured by Keysight N4002ASNS Series Noise Source and Agilent N8975A noise figure analyser (NFA) connected through a bias tee. The measurements are controlled via GPIB. The results between these two methods are compared in Fig.3.11 which shows that they are quite comparable. Since this method is easier and time-saving, the temperature changing experiments will use this 50 Ω method. The GFET and calibration kits are put in the thermal truck in advance. The chamber temperature is cooled down to -60 °C firstly and increased step by step up to -25 °C.

The F_{min} of GFETs in the previous paper are all measured by the source-pull method [17,18]. The 50 Ω method has never been used for GFETs. We take the same F_{50} and S-parameters from the previous paper [17] and calculate the F_{min} and T_{min} using 50 Ω method and compare it with the result in the paper which are measured by source-pull method. Fig.3.11a shows that the T_{min} extracted from the F_{50} is in the range of 200 K to 600 K at the frequency of 2-8 GHz which is approximately the same as that shown in the paper [17]. Fig.3.11b shows the comparison of F_{min} between that calculated by F_{50} and that converted from the T_{min} in paper [17].They are quite consistent with each other which means the F_{50} noise measurement method works as well as the source-pull method for GFET.

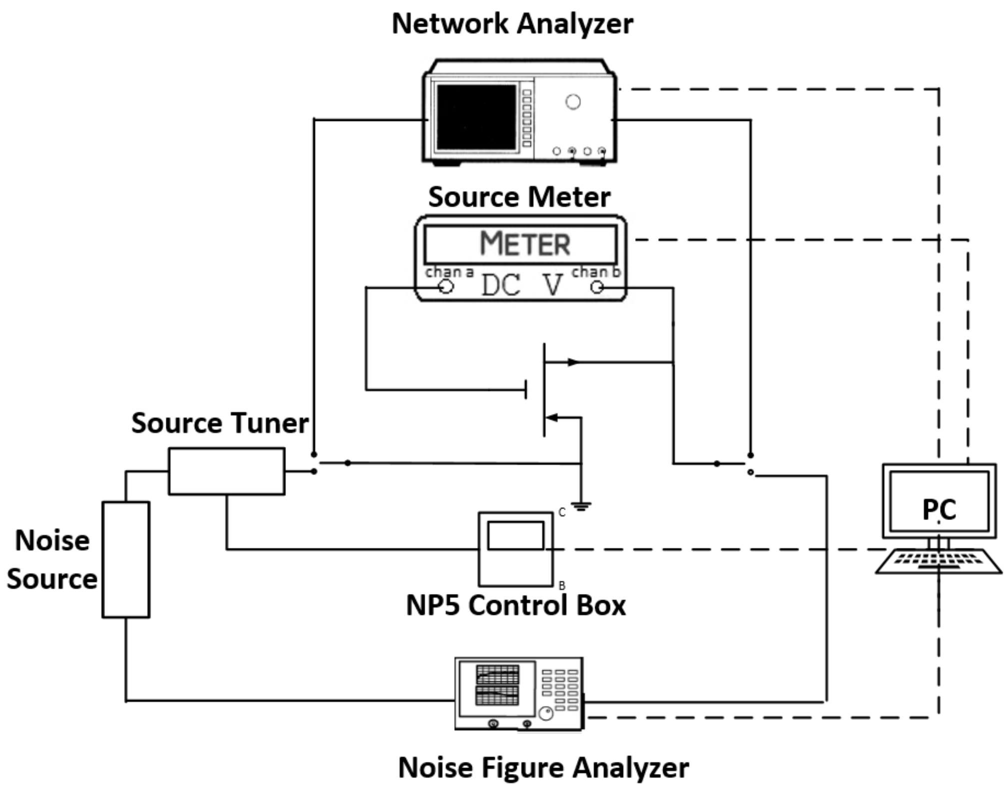

Figure 3.9: Schematic of source-pull noise measurement setup.

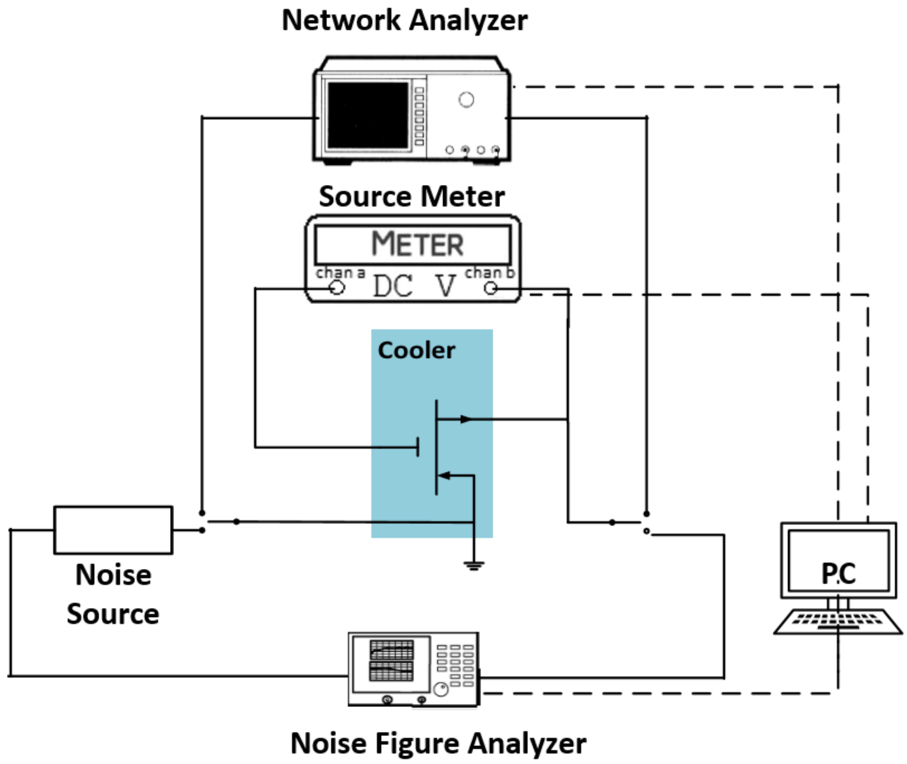

Figure 3.10: Schematic block diagram of noise measurement setup for 50 Ω termination method.

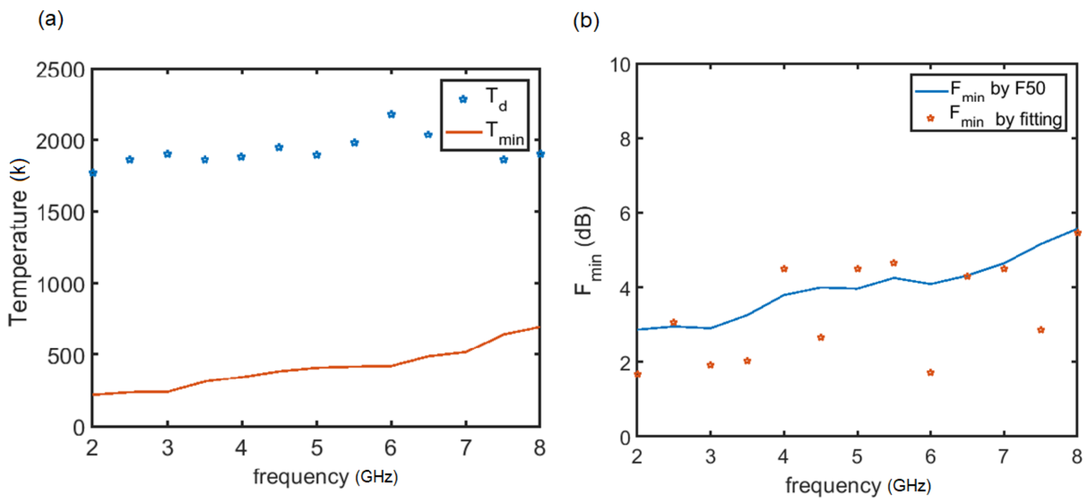

Figure 3.11: (a) T_{min} and T_d calculated from 50 Ohm impedance with the data from the previous paper. (b) F_{min} comparison between source-pull method and 50 Ohm method.

3.4.2 F_{min} at different temperatures and bias voltages

The noise parameters are measured versus bias and frequency at different temperatures. For device A which has no Dirac point shift, the F_{min} versus frequency of 2-18 GHz is shown in Fig.3.12a. It was operated at five different temperatures with the same gate and drain bias. The F_{min} at room temperature is higher than -60 °C as expected, which is partly due to the temperature dependence of the access resistance R_S and R_D. And Fig.3.12b shows that the F_{min} increases approximately linear with the frequency which is consistent with the other FETs.

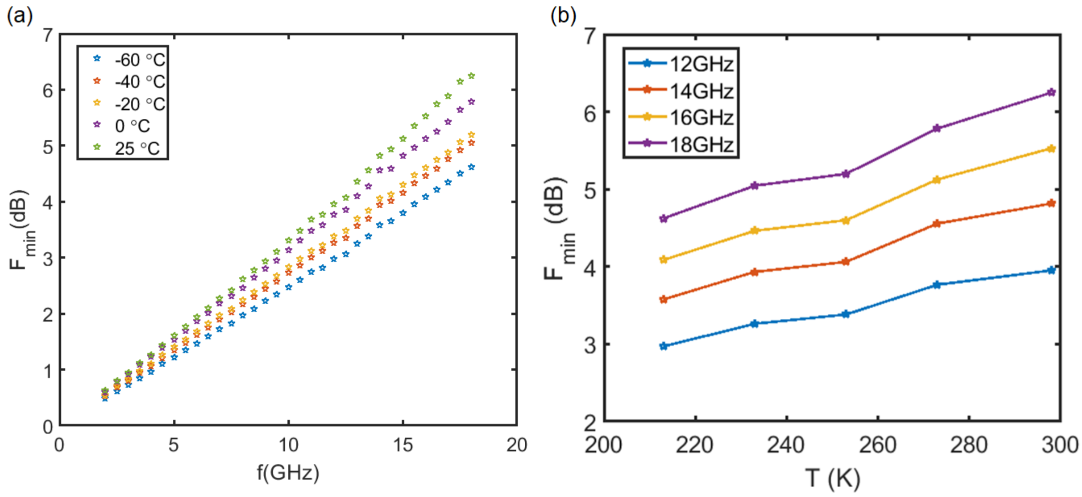

Figure 3.12: (a) F_{min} versus frequency of device A at different temperatures (-60 °C, -40 °C, -20 °C, 0 °C and 25 °C) with gate voltage of -0.1 V and drain voltage of -1.4 V. (b) F_{min} versus temperature of device A for different frequencies (12, 14, 16, and 18 GHz) at gate voltage of -0.1 V and drain voltage of -1.4V.

As we know, the slop of the drain current at very low voltage is an important indicator of the noise performance of a device. From Fig.3.12b we know that the noise is lower at -60 °C compared with room temperature and that is what we can see from the output curves in Fig.3.5a. But it is opposite at cryogenic temperature as shown in Fig.3.5b, which indicates that the noise of graphene transistor at cryogenic temperature is even higher.

the F_{min} increases linearly with frequency, this noise characterisation of GFET is carried out at 6.5 GHz by random and the ambient temperatures range is 237-297 K. The contours of the F_{min} are plotted. The x-axis is the temperature from -60 °C to 25 °C and the Y-axis is the gate voltage. The number on the contour line is the F_{min} in decibel. And these four plots are measured at the drain voltage of -0.8 V, -1 V, -1.2 V and -1.4 V, respectively. With these contour plots, we can see how the noise figure changes with temperature and gate voltage at the same time. And contours of the F_{min} with both drain and gate bias are displayed on Fig.3.14. It shows that F_{min} is relatively stable with drain bias. These plots show that the noise performance of the GFET is insensitive to changes in V_{ds} but very sensitive to V_{gs} and temperature. It is because V_{gs} changes the carrier density while increasing V_{ds} leads to saturation of velocity.

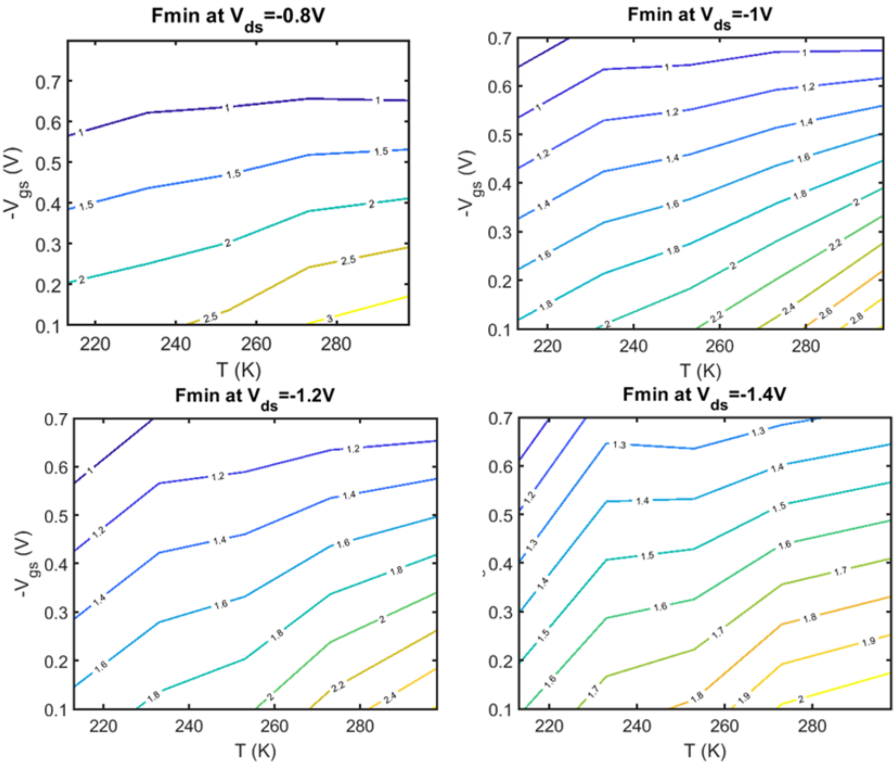

Figure 3.13: F_{min} in decibel of device A versus temperature at 6.5 GHz and drain bias of -0.8, -1, -1.2, -1.4 V respectively

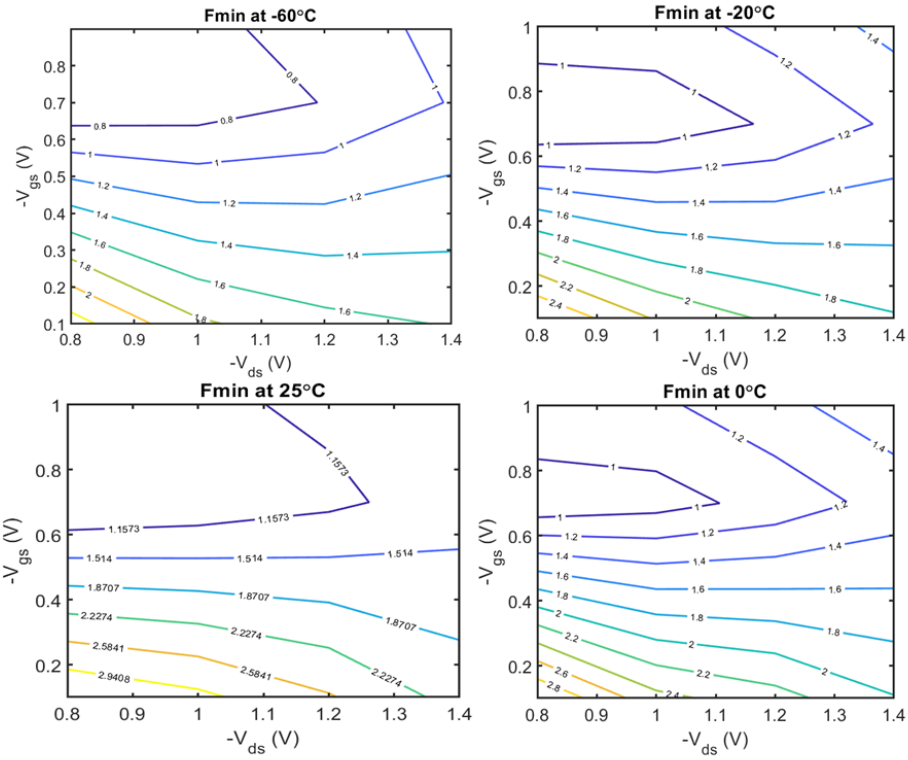

Figure 3.14: F_{min} in decibel of device A versus drain bias at 6.5 GHz and -60, -20, 0, and 25 °C respectively

For comparison, the noise performance of device B is also shown. Fig.3.15a and Fig.3.15b show the F_{min} versus frequency from 2-18 GHz at six different drain voltages with -60 °C and 25 °C, respectively.

Fig.3.16 compares the F_{min} at 4 different temperatures with the same gate and drain bias. And we can see from the Fig.3.16 that at -60 °C the F_{min} is even lower than 1 dB at 18 GHz. And F_{min} at 25 °C is around 2.5 dB for 8 GHz and 4 dB for 18 GHz which is comparable with that published in the previous paper [17, 18].

The Fig.3.17a shows F_{min} versus temperature for different frequencies. It also gives an approximately linear relation. And Fig.3.17b shows that F_{min} will decrease with the drain voltage and saturates above approx. 1 V the same as device A.

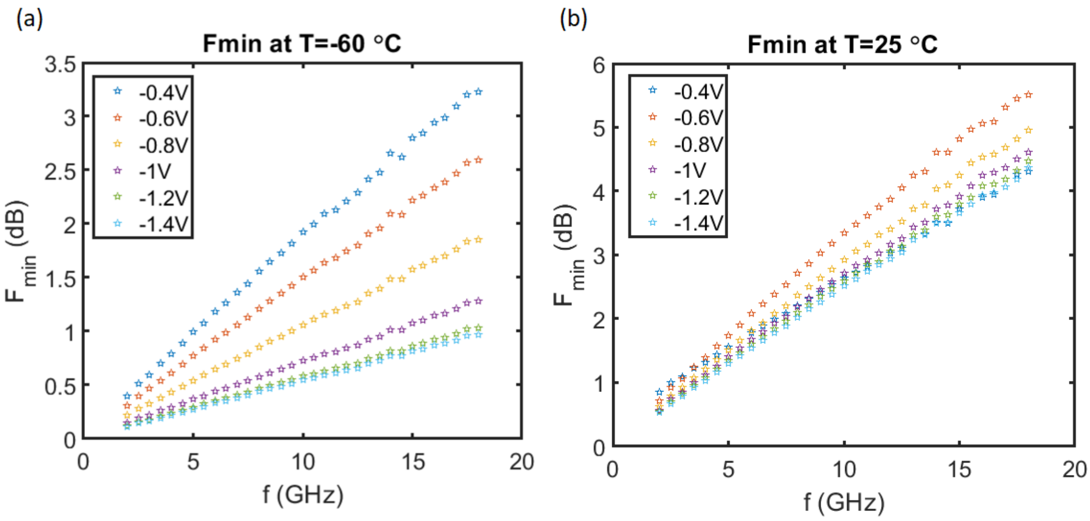

Figure 3.15: F_{min} versus frequency of device B at different drain voltages (-0.4, -0.6, -0.8, -1.2 and -1.4 V), gate voltage of 0.5 V at (a) -60 °C and (b) 25 °C.

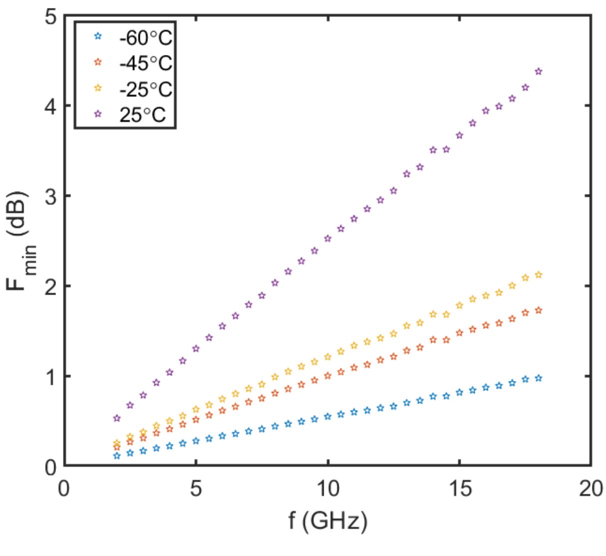

Figure 3.16: F_{min} versus frequency of device B at different temperatures (-60 °C, -45 °C, -25 °C and 25 °C), gate voltage of 0.5 V and drain voltage of -1.4 V.

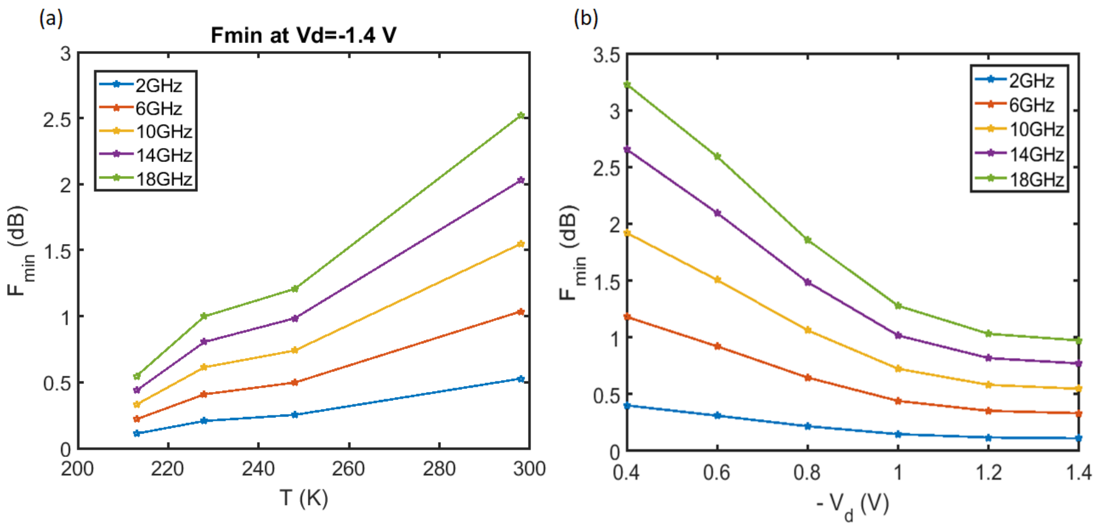

Figure 3.17: (a) F_{min} versus temperature of device B at drain voltage of -1.4V and (b) F_{min} versus drain voltage of device B at ambient temperature of -60 °C, for different frequencies (2, 6, 10, 14 and 18 GHz) at gate voltage of 0.5 V.

Device B has a higher maximum frequency of oscillation (f_{max}) of 18 GHz and 21 GHz at 25 °C and -60 °C respectively. While for device A, the f_{max} is only 14 GHz and 16 GHz for 25 °C and -60 °C respectively. The noise of device B at -60 °C is much lower than device A as shown in Fig.3.18. And the slope of the line which shows the F_{min} versus temperature, device B is larger than device A which means device B is more sensitive to temperature.

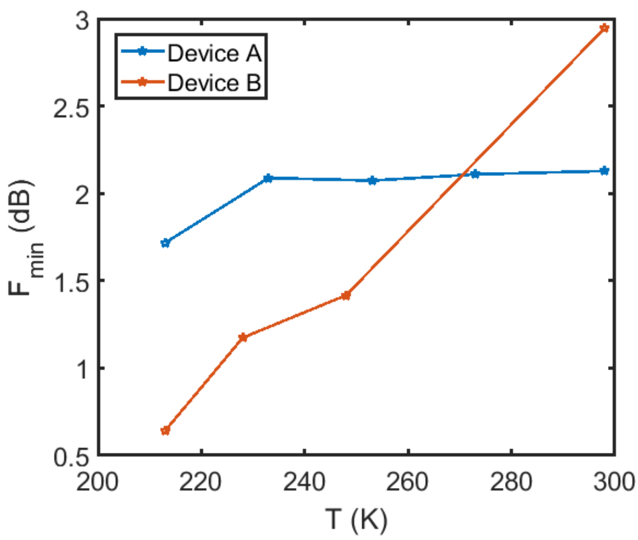

Figure 3.18: F_{min} versus temperature for device A and B at 12 GHz and drain voltage of -1.4 V.

In order to find out which is the key factor of the temperature dependence, the extract parameters fitting from the transfer curves of these two devices are compared in Fig.3.19. The carrier densities n_0 of device B is higher than device A and the carrier mobility μ of device B is lower than device A, but they are almost stable itself versus temperature. The contact resistances R of device A is relatively stable while R of device B fluctuates largely with temperature. This indicates that the contact resistance influences the noise performance with the temperature of a GFET.

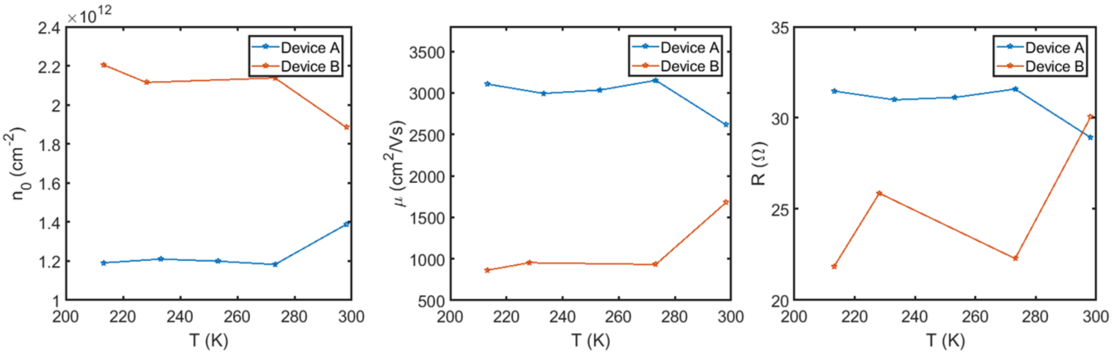

Figure 3.19: (a) The carrier densities n_0, (b) the carrier mobility μ, (c) the contact resistances R versus temperature are fitting from the transfer curves of device A and device B, respectively

3.4.3 Empirical noise model for GFETs

The noise characteristics of the GFET show a large dependence on both temperature and gate voltage. The parasitics extracted at ambient temperature, the temperature of the channel T_{CH} and contact resistance are all temperature-dependent. The access resistances also can be increased due to the self-heating. So we can't keep the assumption that all the parameters are constant versus bias as in the theoretical model. Therefore, it is necessary to extract the temperature and bias dependence of the noise model.

The proposed model is based on a small-signal model with two noise current sources which has temperature and gate voltage dependence. We keep the assumption that the gate temperature is at the ambient temperature. And for our GFET, it has a gate oxide with $I_g < 1$ nA, which is negligible for the noise performance. Therefore we only consider the drain noise current. For the Pospieszalski's noise model, the noise current source i_d increases linearly with frequency. Therefore, it is possible to extract the noise model from measurements at a single frequency. Here we choose it at 6.5 GHz by random. A good low noise bias point is around the maximum point of g_m. Therefore, it is of interest to have a good fit of the model in this gate bias region. This model is derived for gate voltage lower than 1 V and for $V_{ds} = 1.2$ V. The noise at a constant temperature is affected by the gate bias. For different devices, them usually have different Dirac point. Based on the previous results, we assume the noise is approximately linear with the gate bias away from the Dirac point, given by Eq.3.4, where p and q are the fitting parameters that depend on the temperatures. Their quadratic dependence on the temperature in this region is give by Eq.3.5 and Eq.3.6:

Table.3.2 shows the fitting parameters that determines p and q . And then the F_{min} is calculated from the noise current. The modelled and measured results are both shown on the Fig.3.20. The F_{min} decreases with V_{gs} and increases with frequency. This model works very well at the temperature range from -60 °C to 25 °C and gate bias from 0 to -0.8V. This more accurate model can be used in a computer-aided design (CAD) software package and makes it possible to obtain optimum low noise performance at an arbitrary temperature.

$$\frac{i_d}{f} = p\,|V_{gs} - V_{dirac}| + q, \tag{3.4}$$

$$p = a_1 T^2 + a_2 T + a_3, \tag{3.5}$$

$$q = b_1 T^2 + b_2 T + b_3, \tag{3.6}$$

Table 3.2: Fitting parameters of the GFET noise model.

x	1	2	3
a_x	-1.5E-10	4.9E-08	-8.1E-06
b_x	-1.4E-10	9.3E-08	-6.8E-06

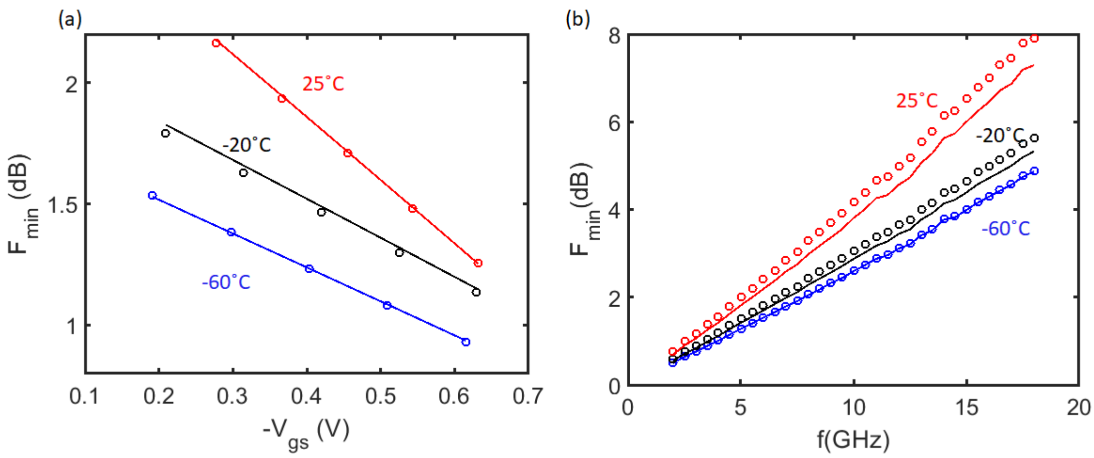

Figure 3.20: Modelled (line) and measured (circle) noise parameters for GFET with $V_{ds} = 1.2$ V (a) at frequency of 6.5 GHz and (b) V_{gs} at -0.1 V with temperature of -60 °C (blue), -20 °C (black) and 25 °C (red), respectively.

4

Conclusion & future work

4.1 Summary

In this thesis, the noise parameters characterisation of GFETs using CVD graphene in the frequency and temperature range of 2 GHz to 18 GHz and -60 °C to 25 °C are demonstrated, respectively. The noise characterisation method combining the cold-source measurement method and 50 Ω termination calculation method is easy for integration in a system with acceptable accuracy. This measurement and calculation method can be used for any other FETs. The GFET with a gate length of 0.75 μm has a f_{max} of 18 GHz and 21 GHz at 25 °C and -60 °C respectively, which is achieved by the use of high-quality graphene in combination with successful optimisation of the GFET fabrication technology, where extreme low source/drain contact resistances were obtained together with reduced parasitic pad capacitances [50]. This gives the GFET a F_{min} of 1.2 dB at 6.5 GHz and 25 °C which is comparable with that from previous source-pull method [17, 18], and that of the best MESFET [52]. And the F_{min} decreases down to 0.3 dB at 8 GHz and -60 °C and increases almost linearly with temperature at a certain frequency. The rather large temperature dependence seen for contact resistance has a large effect on the noise performance at this temperature range. This effect can be taken into account for designing graphene LNAs. The F_{min} increases with the V_{gs} is due to the carrier density enhancement. And the F_{min} decreases with the drain voltage and saturates above approximate 1 V which is most likely due to the carrier velocity saturation. The relatively stable noise performance above V_{ds} of 1 V allows designer to optimise for gain by increasing V_{ds} a bit in this region. The proposed empirical noise model for the GFET considering both temperature and gate voltage influence is based on the small-signal model and Pospieszalski's noise model. This model can be applied in the temperature from -60 °C to 25 °C and gate bias of -0.8 - 0 V.

4.2 Outlook

The knowledge of noise parameters at different ambient temperatures obtained from this thesis paves the way for the design of graphene LNA. However, the noise at the cryogenic temperature might have a different performance as shown in the output curves, which means the proposed noise model has a temperature range limitation. To develop a more accurate model, the cryogenic noise characterisation and the causes of the unexpected dc curves at cryogenic temperature still need to be investigated. The noise performance of the GFETs measured in this work can be comparable with Si CMOS and MESFET, but it still needs to be improved to be comparable with GaAs or InP HEMTs [53, 54]. The f_T and f_{max} also need to be increased in order to extend to higher frequencies. The f_T and f_{max} are not as high as the expectation which is because the carrier mobility in graphene doesn't reach the expectation in the theory. This is due to the impurity introduced during fabrication. Some methods have been proposed to solve it, such as using hexagonal boron nitride (hBN) capsulation by an advanced dry van-der Waals transfer method [55]. For the structure, the gate width can be lager to increase the capacitance and the gate length can be shorter by using T-shape to decrease the contact resistance [56]. Consequently, it will provide GFETs with a better noise performance.

Bibliography

[1] P. H. Siegel, "Terahertz technology in biology and medicine," *IEEE Transactions on Microwave Theory and Techniques*, vol. 52, no. 10, pp. 2438–2447, Oct 2004. doi: 10.1109/TMTT.2004.835916

[2] R. Appleby and R. N. Anderton, "Millimeter-wave and submillimeter-wave imaging for security and surveillance," *Proceedings of the IEEE*, vol. 95, no. 8, pp. 1683–1690, Aug 2007. doi: 10.1109/JPROC.2007.898832

[3] S. Rangan, T. S. Rappaport, and E. Erkip, "Millimeter-wave cellular wireless networks: Potentials and challenges," *Proceedings of the IEEE*, vol. 102, no. 3, pp. 366–385, March 2014. doi: 10.1109/JPROC.2014.2299397

[4] W. Shockley, "A unipolar "field-effect" transistor," *Proceedings of the IRE*, vol. 40, no. 11, pp. 1365–1376, Nov 1952. doi: 10.1109/JRPROC.1952.273964

[5] T. Mimura, "The early history of the high electron mobility transistor (HEMT)," *Microwave Theory and Techniques, IEEE Transactions on*, vol. 50, pp. 780 – 782, 04 2002. doi: 10.1109/22.989961

[6] L. A. Samoska, "An overview of solid-state integrated circuit amplifiers in the submillimeter-wave and THz regime," *IEEE Transactions on Terahertz Science and Technology*, vol. 1, no. 1, pp. 9–24, Sep. 2011. doi: 10.1109/TTHZ.2011.2159558

[7] K. S. Novoselov, A. K. Geim, S. V. Morozov, D. Jiang, Y. Zhang, S. V. Dubonos, I. V. Grigorieva, and A. A. Firsov, "Electric field effect in atomically thin carbon films," *Science*, vol. 306, no. 5696, pp. 666–669, 2004. doi: 10.1126/science.1102896

[8] K. Bolotin, K. Sikes, Z. Jiang, M. Klima, G. Fudenberg, J. Hone, P. Kim, and H. Stormer, "Ultrahigh electron mobility in suspended graphene," *Solid State Communications*, vol. 146, no. 9, pp. 351 – 355, 2008. doi: 10.1016/j.ssc.2008.02.024

[9] M. C. Lemme, T. J. Echtermeyer, M. Baus, and H. Kurz, "A graphene field-effect device," *IEEE Electron Device Letters*, vol. 28, no. 4, pp. 282–284, April 2007. doi: 10.1109/LED.2007.891668

[10] F. Schwierz, "Graphene transistors," *Nature Nanotechnology*, vol. 5, p. 487, 2010. doi: 10.1038/nnano.2010.89

[11] X. Yang, A. Vorobiev, A. Generalov, M. A. Andersson, and J. Stake, "A flexible graphene terahertz detector," *Applied Physics Letters*, vol. 111, no. 2, p. 021102, 2017. doi: 10.1063/1.4993434

[12] M. S. Gupta, "Power gain in feedback amplifiers, a classic revisited," *IEEE Transactions on Microwave Theory and Techniques*, vol. 40, no. 5, pp. 864–879, May 1992. doi: 10.1109/22.137392

[13] S. J. Mason, "Feedback theory-some properties of signal flow graphs," *Proceedings of the IRE*, vol. 41, no. 9, pp. 1144–1156, Sep. 1953. doi: 10.1109/JRPROC.1953.274449

[14] F. Schwierz, "Graphene transistors: Status, prospects, and problems," *Proceedings of the IEEE*, vol. 101, no. 7, pp. 1567–1584, July 2013. doi: 10.1109/JPROC.2013.2257633

[15] M.Andersson., "Characterisation and modelling of graphene FETs for terahertz mixers and detectors." *Chalmers Doctor thesis*, 2016.

[16] M. A. Andersson, O. Habibpour, J. Vukusic, and J. Stake, "10 dB small-signal graphene FET amplifier," *Electronics Letters*, vol. 48, no. 14, pp. 861–863, July 2012. doi: 10.1049/el.2012.1347

[17] M. Tanzid, M. A. Andersson, J. Sun, and J. Stake, "Microwave noise characterization of graphene field effect transistors," *Applied Physics Letters*, vol. 104, no. 1, p. 013502, 2014. doi: 10.1063/1.4861115

[18] C. Yu, Z. Z. He, X. B. Song, Q. B. Liu, S. B. Dun, T. T. Han, J. J. Wang, C. J. Zhou, J. C. Guo, Y. J. Lv, S. J. Cai, and Z. H. Feng, "High-frequency noise characterization of graphene field effect transistors on SiC substrates," *Applied Physics Letters*, vol. 111, no. 3, p. 033502, 2017. doi: 10.1063/1.4994324

[19] C.-H. Yeh, Y.-W. Lain, Y.-C. Chiu, C.-H. Liao, D. Ricardo Moyano, S. S H Hsu, and P.-W. Chiu, "GHz flexible graphene transistors for microwave integrated circuits." *ACS nano*, vol. 8, 07 2014. doi: 10.1021/nn5036087

[20] A. J. Scholten, L. F. Tiemeijer, R. van Langevelde, R. J. Havens, A. T. A. Zegers-van Duijnhoven, and V. C. Venezia, "Noise modeling for RF CMOS circuit simulation," *IEEE Transactions on Electron Devices*, vol. 50, no. 3, pp. 618–632, March 2003. doi: 10.1109/TED.2003.810480

[21] Jung-Suk Goo, Chang-Hoon Choi, E. Morifuji, H. S. Momose, Zhiping Yu, H. Iwai, T. H. Lee, and R. W. Dutton, "RF noise simulation for submicron MOSFET's based on hydrodynamic model," in *1999 Symposium on VLSI Technology. Digest of Technical Papers (IEEE Cat. No.99CH36325)*, June 1999. doi: 10.1109/VLSIT.1999.799389 pp. 153–154.

[22] J. Wenger, "Quarter-micrometer low-noise pseudomorphic GaAs HEMTs with extremely low dependence of the noise figure on drain-source current," *IEEE Electron Device Letters*, vol. 14, no. 1, pp. 16–18, Jan 1993. doi: 10.1109/55.215086

[23] P. Ho, P. C. Chao, K. H. G. Duh, A. A. Jabra, J. M. Ballingall, and P. M. Smith, "Extremely high gain, low noise InAlAs/InGaAs HEMTs grown by molecular beam epitaxy," pp. 184–186, Dec 1988. doi: 10.1109/IEDM.1988.32785

[24] G. Gonzalez, *Microwave Transistor Amplifiers: Analysis and Design*. Prentice Hall, 1997. ISBN 9780132543354. [Online]. Available: https://books.google.se/books?id=-AVTAAAAMAAJ

[25] J. B. Johnson, "Thermal agitation of electricity in conductors," *Phys. Rev.*, vol. 32, pp. 97–109, Jul 1928. doi: 10.1103/PhysRev.32.97

[26] H. Nyquist, "Thermal agitation of electric charge in conductors," *Phys. Rev.*, vol. 32, pp. 110–113, Jul 1928. doi: 10.1103/PhysRev.32.110

[27] G. H. Hanson and A. V. Der Ziel, “Shot noise in transistors,” *Proceedings of the IRE*, vol. 45, no. 11, pp. 1538–1542, Nov 1957. doi: 10.1109/JRPROC.1957.278349

[28] V. Mitin, L. Reggiani, and L. Varani., “Noise and fluctuations control in electronic devices.” *American Scientific Publishers*, 2002.

[29] S. Maas., “Noise in linear and nonlinear circuits.” *Artech House*, 2005.

[30] H. T. Friis, “Noise figures of radio receivers,” *Proceedings of the IRE*, vol. 32, no. 7, pp. 419–422, July 1944. doi: 10.1109/JRPROC.1944.232049

[31] H. Fukui, “Available power gain, noise figure, and noise measure of two-ports and their graphical representations,” *IEEE Transactions on Circuit Theory*, vol. 13, no. 2, pp. 137–142, June 1966. doi: 10.1109/TCT.1966.1082556

[32] F. Schwierz and J. Liou., “Modern microwave transistors: Theory, design and performance.” *Hoboken, New Jersey: John Wiley and Sons*, 2003.

[33] M. Pospieszalski, “Modeling of noise parameters of MESFETs and MODFETs and their frequency and temperature dependence,” *Microwave Theory and Techniques, IEEE Transactions on*, vol. 37, pp. 1340–1350, 09 1989. doi: 10.1109/22.32217

[34] H. Rothe and W. Dahlke, “Theory of noisy fourpoles,” *Proceedings of the IRE*, vol. 44, no. 6, pp. 811–818, June 1956. doi: 10.1109/JRPROC.1956.274998

[35] M. Pospieszalski, “Interpreting transistor noise.” *Microwave Magazine, IEEE*, vol. 11, pp. 61 – 69, 2010.

[36] M. A. Andersson and J. Stake, “An accurate empirical model based on volterra series for FET power detectors,” *IEEE Transactions on Microwave Theory and Techniques*, vol. 64, no. 5, pp. 1431–1441, May 2016. doi: 10.1109/TMTT.2016.2532326

[37] K. Technologies, “Fundamentals of rf and microwave noise figure measurements.” *Keysight Technologies Application note.*

[38] N. Otegi, J. M. Collantes, and M. Sayed, “Cold-source measurements for noise figure calculation in spectrum analyzers,” in *2006 67th ARFTG Conference*, June 2006. doi: 10.1109/ARFTG.2006.4734387 pp. 223–228.

[39] D. M. Pozar., “Microwave engineering, 4th edition.” *Wiley Global Education US*, vol. 11, 2011.

[40] P. J. Tasker, W. Reinert, J. Braunstein, and M. Schlechtweg, “Direct extraction of all four transistor noise parameters from a single noise figure measurement,” in *1992 22nd European Microwave Conference*, vol. 1, 09 1992. doi: 10.1109/EUMA.1992.335733 pp. 157–162.

[41] G. Dambrine, H. Happy, F. Danneville, and A. Cappy, “A new method for on wafer noise measurement,” *IEEE Transactions on Microwave Theory and Techniques*, vol. 41, no. 3, pp. 375–381, March 1993. doi: 10.1109/22.223734

[42] B. Hughes, “A temperature noise model for extrinsic FETs,” *IEEE Transactions on Microwave Theory and Techniques*, vol. 40, no. 9, pp. 1821–1832, Sep. 1992. doi: 10.1109/22.156610

[43] M. Berroth and R. Bosch, “Broad-band determination of the FET small-signal equivalent circuit,” *IEEE Transactions on Microwave Theory and Techniques*, vol. 38, no. 7, pp. 891–895, 07 1990. doi: 10.1109/22.55781

[44] G. Dambrine, A. Cappy, F. Heliodore, and E. Playez, "A new method for determining the FET small-signal equivalent circuit," *IEEE Transactions on Microwave Theory and Techniques*, vol. 36, no. 7, pp. 1151–1159, July 1988. doi: 10.1109/22.3650

[45] M. Yi and Z. Shen, "A review on mechanical exfoliation for the scalable production of graphene," *J. Mater. Chem. A*, vol. 3, pp. 11 700–11 715, 2015. doi: 10.1039/C5TA00252D

[46] G. Deokar, J. Avila, I. Razado-Colambo, J.-L. Codron, C. Boyaval, E. Galopin, M.-C. Asensio, and D. Vignaud, "Towards high quality CVD graphene growth and transfer," *Carbon*, vol. 89, pp. 82 – 92, 2015. doi: 10.1016/j.carbon.2015.03.017

[47] C. Berger, Z. Song, X. Li, X. Wu, N. Brown, C. Naud, D. Mayou, T. Li, J. Hass, A. N. Marchenkov, E. H. Conrad, P. N. First, and W. A. de Heer, "Electronic confinement and coherence in patterned epitaxial graphene," *Science*, vol. 312, no. 5777, pp. 1191–1196, 2006. doi: 10.1126/science.1125925

[48] J. Kedzierski, P. Hsu, P. Healey, P. Wyatt, and C. Keast, "Epitaxial graphene transistors on SiC substrates," in *2008 Device Research Conference*, June 2008. doi: 10.1109/DRC.2008.4800720. ISSN 1548-3770 pp. 25–26.

[49] S. Bidmeshkipour, A. Vorobiev, M. A. Andersson, A. Kompany, and J. Stake, "Effect of ferroelectric substrate on carrier mobility in graphene field-effect transistors," *Applied Physics Letters*, vol. 107, no. 17, p. 173106, 2015. doi: 10.1063/1.4934696

[50] M. Bonmann, M. Asad, X. Yang, A. Generalov, A. Vorobiev, L. Banszerus, C. Stampfer, M. Otto, D. Neumaier, and J. Stake, "Graphene field-effect transistors with high extrinsic f_T and $f_{\max}$," *IEEE Electron Device Letters*, vol. 40, no. 1, pp. 131–134, Jan 2019. doi: 10.1109/LED.2018.2884054

[51] S. Kim, J. Nah, I. Jo, D. Shahrjerdi, L. Colombo, Z. Yao, E. Tutuc, and S. K. Banerjee, "Realization of a high mobility dual-gated graphene field-effect transistor with Al2O3 dielectric," *Applied Physics Letters*, vol. 94, no. 6, p. 062107, 2009. doi: 10.1063/1.3077021

[52] Z. Ramezani, A. A. Orouji, and M. Rahimian, "High-performance SOI MESFET with modified depletion region using a triple recessed gate for RF applications," *Materials Science in Semiconductor Processing*, vol. 30, pp. 75 – 84, 2015. doi: 10.1016/j.mssp.2014.09.023

[53] J. Wenger, "Quarter-micrometer low-noise pseudomorphic GaAs HEMTs with extremely low dependence of the noise figure on drain-source current," *IEEE Electron Device Letters*, vol. 14, no. 1, pp. 16–18, Jan 1993. doi: 10.1109/55.215086

[54] J. Schleeh, G. Alestig, J. Halonen, A. Malmros, B. Nilsson, P. A. Nilsson, J. P. Starski, N. Wadefalk, H. Zirath, and J. Grahn, "Ultralow-power cryogenic InP HEMT with minimum noise temperature of 1 K at 6 GHz," *IEEE Electron Device Letters*, vol. 33, no. 5, pp. 664–666, May 2012. doi: 10.1109/LED.2012.2187422

[55] L. Banszerus, M. Schmitz, S. Engels, M. Goldsche, K. Watanabe, T. Taniguchi, B. Beschoten, and C. Stampfer, "Ballistic transport exceeding 28 μ m

in CVD grown graphene," *Nano letters*, vol. 16, p. 1387, 01 2016. doi: 10.1021/acs.nanolett.5b04840

[56] E. Cha, G. Moschetti, N. Wadefalk, P. Nilsson, S. Bevilacqua, A. Pourkabirian, P. Starski, and J. Grahn, "Two-finger InP HEMT design for stable cryogenic operation of ultra-low-noise Ka- and Q-band LNAs," *IEEE Transactions on Microwave Theory and Techniques*, vol. 65, no. 12, pp. 5171–5180, Dec 2017. doi: 10.1109/TMTT.2017.2765318

A

Matlab code

The MATLAB files for analysis of F_{min} are encoded.

A.1 Main file

```

%% Noise parameter characterization
instrreset ;
clear all ;
close all ;
clc ;
path(path,'code') ;

%% Setup

% measurement frequency

setup. fstart = 2; % start frequency in GHz
setup. fstop = 18; % stop frequency in GHz
setup. fstep = .5; % step frequency in GHz

% delay in through standard

setup.delay=0;
data.freq = 2:.5:18;
freq = 2:.5:18;

% ENR of the reference noise source

NoiseSourceFile = 'enr';

setup.averaging = 8; % number of averages done, 1 - 512
setup.rf_atten = 30; % rf attenuation setting (1 - 6), 0 = auto
setup.if_atten = 0;

% vna settings Anritsu
setup.vna_start = setup.fstart.*1e3;
setup.vna_step = setup.fstep.*1e3;
setup.vna_points = length(data.freq);
setup.vna_pwr = -10;
setup.vna_att1 = 20;
setup.vna_att2 = 20;
setup.vna_IFBW = 'IF1';% 'IF1'=10 Hz,'IF2'=100 Hz 'IF3'=1000 Hz 'IF4'=10000 Hz
```

```
setup.DutCalset = 2;
setup.GsCalset = 3;
setup.GlCalset = 4;

%% Initilize measurement system
 instr = init_atn_nfa(setup);


%% perform noise port calibration
input('Connect through at DUT plane');
Calibration = NoisePortCal_onwafer(instr);

%% Read 50 ohm hot cold noise
input('Connect noise source for 50ohm reference measurement and press ENTER');
[Calibration.G0kdf setup] = NoiseRef_nfa_sweep(instr, setup);
save('data/calibration_cal','Calibration');

%% Connect the DUT to the VNA
% turn on vna
vna = get(instr.vna, 'Interface');
 fprintf(vna, 'SINC;S22;DRIVPORT2');
 fprintf(get(instr.vna,'interface'), 'AVG 512');
 fprintf(get(instr.vna,'interface'), 'AVG 32');

% turn off vna
 fprintf(vna, 'S22;DRIVNONE');

%% Fix WinCal
WinCalFix(instr.vna, setup);

%% Correct noise port calibration
[ns_gamma inputS] = NoisePortCorrection_onwafer(instr, Calibration, setup);
Calibration.ns_gamma = ns_gamma;
Calibration.inputS = inputS;
save('data/calibration','Calibration');

%% perform nfm gamma calibration
% input('Connect thru at DUT plane');
disp('Measures the gamma of receiver presented to dut');
Calibration.nfm_gamma = NFM_Gamma_onwafer(instr, setup);
save('data/calibration','Calibration');

%%
% measure gammas presented to the DUT
Calibration.GammaS = GammaSCal_onwafer(probe, carridge, instr, setup);
save('data/calibration', 'Calibration');

% perform recevier nosie parameter calibration
% input('Connect noise source and press ENTER');
[Calibration.RecNoise setup] = NoiseCal_nfa(Calibration, instr, setup);
save('data/calibration', 'Calibration');
% tmp = CorrectNoiseMeasure(RecNoise, G0kdf, ns_gamma, freq);

% calculate noise parameters of receiver
load(NoiseSourceFile);
Calibration.Ta = 25; Calibration.Z0 = 50;
```

```
enr2.freq  = data.freq;
enr2.data = interp1(enr.freq, enr.data, enr2.freq);
ReceiverNoise = CalculateReceiverNoise_onwafer(Calibration, enr2);

save('data/ReceiverNoise', 'ReceiverNoise');


%% perform dut noise parameter measurement
input('Connect DUT and press ENTER');
[noiseDut setup] = MeasDUTNoise(Calibration, instr, setup);
save('data/DUTMeas', 'noiseDut');

%% calculate noise parameters of DUT
NP = CalculateDUTNoise(noiseDut, Calibration, ReceiverNoise);
save('data/DUTNP', 'NP');
```

B

Conference paper

High frequency noise characterisation of graphene field-effect transistors at different temperatures

Junjie Li, Xinxin Yang, Marlene Bonmann, Muhammad Asad, Andrei Vorobiev, Jan Stake, Luca Banszerus, Christoph Stampfer, Martin Otto, Daniel Neumaier

In Graphene Week Conference, Helsinki, Finland, 2019.

High frequency noise characterisation of graphene field-effect transistors at different temperatures

Junjie Li[1], Xinxin Yang[1], Marlene Bonmann[1], Muhammad Asad[1], Andrei Vorobiev[1], Jan Stake[1], Luca Banszerus[2], Christoph Stampfer[2], Martin Otto[3], Daniel Neumaier[3]

[1]*Terahertz and Millimetre Wave Laboratory, Department of Microtechnology and Nanoscience, Chalmers University of Technology, SE-41296 Gothenburg, Sweden,*
[2]*2nd Institute of Physics, RWTH Aachen University, 52074 Aachen, Germany,*
[3]*Advanced Microelectronic Center Aachen, AMO GmbH, 52074, Aachen, Germany*

Graphene is a promising material for high frequency electronics applications thanks to its intrinsically high carrier mobility and velocity, and graphene transistors are continuously pushed toward higher operating frequencies [1]. For high frequency low noise amplifiers, it is important to evaluate the noise parameters of the graphene field-effect transistors (GFETs). In this work, we present the noise performance of the GFETs made of chemical vapour deposition (CVD) in the frequency and temperature ranges of 2-18 GHz and -60-25 °C. The noise figure with 50 Ω impedance termination (F_{50}) was measured using the cold-source method and then the minimum noise figure (F_{min}) was estimated using the Pospieszalski's noise model [2, 3]. In Fig. 1 and Fig. 2, the F_{min} of a GFET with a gate length of 0.5 µm as a function of the frequency (f) and drain voltage (V_d) at different temperatures are shown. This GFET revealed maximum frequency of oscillation (f_{max}) of 18 and 21 GHz at 25 and -60 °C, respectively. It can be seen from Fig. 1, that the F_{min} at 8 GHz is approx. 2 dB lower than that of the previously published CVD GFETs and comparable with that of the best published SiC GFETs [4, 5]. The F_{min} decreases significantly with temperature down to 0.3 dB at 8 GHz, competing with Si CMOS [6]. It can be seen from Fig. 2, that F_{min} decreases with the V_d and saturates above approx. 1 V, where GFETs operate in the velocity saturation mode [1]. Analysis of the dependences allows for further development of the GFETs for advanced low noise amplifiers.

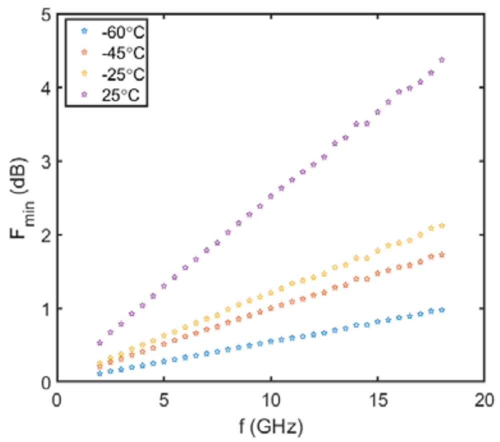

Fig. 1. F_{min} versus frequency at different temperatures (-60, -45, -25 and 25 °C), gate voltage of 0.5 V and drain voltage of -1.4 V.

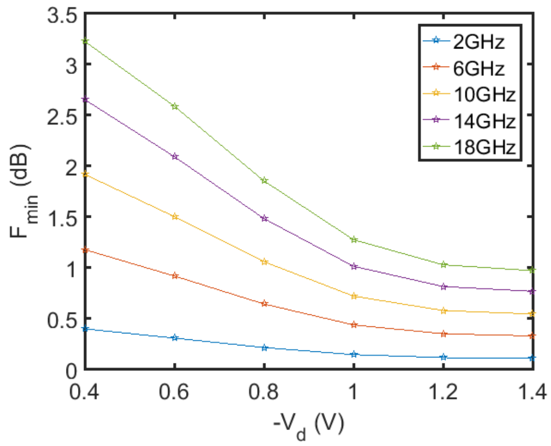

Fig. 2. F_{min} versus drain voltage at temperature of -60°C for different frequencies (2, 6, 10, 14 and 18 GHz) at gate voltage of 0.5 V.

References

[1] M. Bonmann, M. Asad and X. Yang et al., *IEEE Electron Device Lett.* , 40 (1), 131 (2019).
[2] M. W.Pospieszalski, *IEEE Trans. Microw. Theory Tech*., 37 (9), 3476840 (1989)
[3] P. J. Tasker, W. Reinert and J. Braunstein et al., *European Microwave Conference*, 157–162 (1992).
[4] M. Tanzid, M. A. Andersson and J. Sun, et al., *Appl. Phys. Lett*., 104 (1), 013502 (2014)
[5] C. Yu, Z. Z. He, X. B. Song et al., *Appl. Phys. Lett*., 111 (3), 033502 (2017);
[6] L. Belostotski, J. W. Haslett, *IEEE Solid-State Circuits Lett.* , 42 (11), 9671178, (2007)